Spatial Variations of the Wave, Stress and Wind Fields in the Shoaling Zone

Larry Mahrt

College of Oceanic and Atmospheric Sciences

Oregon State University

Corvallis, OR 97331

phone: (541) 737-5691   fax: (541) 737-2540   email: mahrt@coas.oregonstate.edu

Grant#: N000149710279

http:blg.oce.orst.edu/shoaling

FINAL REPORT
2 SEPTEMBER 2003

REPORT DOCUMENTATION PAGE

Form Approved
OMB No. 0704-0188

1. AGENCY USE ONLY (Leave blank)	2. REPORT DATE 9-02-03	3. REPORT TYPE AND DATES COVERED 2-01-97 to 9-30-03

4. TITLE AND SUBTITLE
Spatial Variations of the Wave, Stress and Wind Fields in the Shoaling Zone

5. FUNDING NUMBERS
N00014-97-1-0279

6. AUTHOR(S)
Larry Mahrt

7. PERFORMING ORGANIZATION NAME(S) AND ADDRESS(ES)
OSU
Corvallis, OR 97331

8. PERFORMING ORGANIZATION REPORT NUMBER
N00898

9. SPONSORING/MONITORING AGENCY NAME(S) AND ADDRESS(ES)
ONR

10. SPONSORING/MONITORING AGENCY REPORT NUMBER

11. SUPPLEMENTARY NOTES

12a. DISTRIBUTION/AVAILABILITY STATEMENT
Unlimited Public Access

12b. DISTRIBUTION CODE

13. ABSTRACT (Maximum 200 words)

Abstract. Aircraft data collected at approximately 15 m above the sea surface in the coastal zone are analyzed to examine the spatial distribution of surface stress. Advection of stronger turbulence from land dominates the near-surface turbulence for the first few kilometers offshore. With offshore flow of warm air over cold water, strong stratification leads to very small surface stress. Because the stability restricts the momentum transfer to the waves, the aerodynamic surface roughness decreases to very small values, which in turn decreases atmospheric mixing. The redevelopment of the boundary layer farther downstream is examined. Computation of fluxes from observations for stable cases is difficult due to a variety of errors including large random flux errors, possible instrumental loss of small-scale flux, difference between the surface flux and that at the observational level, and inadvertent capture of mesoscale motions in the computed turbulent fluctuations. Although the errors appear to be substantial, the aircraft momentum fluxes compare favorably with those from sonic anemometers on two buoys and a tower at the end of a 570-m pier, even with near collapse of the turbulence.

14. SUBJECT TERMS

15. NUMBER OF PAGES

16. PRICE CODE

17. SECURITY CLASSIFICATION OF REPORT	18. SECURITY CLASSIFICATION OF THIS PAGE	19. SECURITY CLASSIFICATION OF ABSTRACT	20. LIMITATION OF ABSTRACT

Spatial Variations of the Wave, Stress and Wind Fields in the Shoaling Zone

Larry Mahrt

College of Oceanic and Atmospheric Sciences

Oregon State University

Corvallis, OR 97331

phone: (541) 737-5691   fax: (541) 737-2540 email: mahrt@coas.oregonstate.edu

Grant#: N000149710279

http:blg.oce.orst.edu/shoaling

FINAL REPORT
2 SEPTEMBER 2003

Spatial Variations of the Wave, Stress and Wind Fields in the Shoaling Zone

Final report

Larry Mahrt
College of Oceanic and Atmospheric Sciences
Oregon State University
Corvallis, OR 97331
phone: (541) 737-5691   fax: (541) 737-2540   email: mahrt@coas.oregonstate.edu
Grant #: N000149710279
http://blg.oce.orst.edu/shoaling

LONG-TERM GOAL

The long term goal was to improve physical understanding of sea surface fluxes and atmospheric boundary layer development in the coastal zone, improve formulation of surface fluxes and implement the revised formulations into regional and large-scale models.

OBJECTIVES

The objectives were to generalize parameterization of the aerodynamic roughness length without inclusion of a full wave model, extend these improvements to heat and moisture transport and set the framework for inclusion of information on wave state.

APPROACH

The primary approach is to re-analyze eddy correlation data from SHOWEX and RASEX and incorporate additional data sets from NPS buoys in SHOWEX and near Wallops Island and offshore tower data from the University of Uppsala. Cooperative modeling efforts will be carried out with Scott Sandgathe, Phil Barbour and Roger Samelson at OSU using COAMPS.

RESULTS

Here, we survey results from six major studies conducted with funds from this grant. For the data sets outlined above, the usual formulations for the aerodynamic roughness length based on the Charnock relationship and wave age are dominated by artificial self-correlation. The physical variance explained is small. This dominance remains even after removing cases with short fetch, weak winds and upward momentum flux from the sea surface. In addition, the overall behavior of the Charnock coefficient is sensitive to the treatment of numerous outliers and the method for averaging values of the roughness length over the various records. Part of the large variability of the Charnock coefficient is due to the influence of wave state. Relationships allowing the dependence of the Charnock coefficient on wave age are still dominated by self-correlation. However, inclusion of information on the significant wave height does increase the physical variance explained.

The extreme variability of the Charnock coefficient is also due to anomalously low values in very stable conditions as well as observational problems and deviations from Monin-Obukhov similarity theory, all of which is absorbed in the "backed out" aerodynamic roughness length. Winds following the swell lead to very small values of the aerodynamic roughness length and Charnock coefficient although these results are based on a small subset of the data and require much more careful examination.

Unfortunately, most regional and large-scale models cannot accommodate the complexity and computer time required for a full wave model. Formulations based on the Charnock coefficient will probably remain a primary parameterization for closing the surface stress formulation in numerical models even if assigning physical significance to these relationships is tenuous. Collectively summarizing the present data sets suggests using a smaller value of the Charnock coefficient at intermediate wind speeds compared to traditional values of the Charnock coefficient. Restricting the data set further by excluding frequent swell conditions, improves the performance of the simple formulations but swell conditions are common in the coastal zone.

A formulation for the dependence of the Charnock coefficient on wind speed has been developed as a pragmatic "poor man" substitute for information on wave state and other influences causing deviations from Monin-Obukhov similarity theory. Although a substantial improvement upon the specification of a constant Charnock coefficient, this formulation cannot account for major aspects of the influence of wave state and is physically indirect and incomplete.

We have studied the impact of errors due to vertical displacement of platforms resulting from contamination of the computed turbulent fluctuations by mean vertical gradients using LongEZ and ASIS buoy data. Aircraft platform fluctuations for the present data lead to small overestimation of the heat and momentum fluxes for stable conditions and unimportant errors for unstable conditions. For typical record lengths, the magnitude of the displacement flux error is generally smaller than the usual random flux error, where the latter remains nonzero even for stationary platforms. Both random errors are reduced by increasing record length.

The displacement flux error can be theoretically partitioned into a random part (not to be confused with the usual random flux error) and a systematic part. The flux displacement error for short aircraft records is strongly influenced by the random part of the displacement flux error, which is smaller than the usual random flux error. For longer aircraft records, the random part of the displacement flux error decreases and the displacement flux error approaches the small systematic part of the error, typically a few percent of the total flux for stable conditions and less than one percent for unstable conditions. The systematic error tends to increase with stability. The general unimportance of the displacement error for the LongEZ is encouraging since this small aircraft is displaced more by atmospheric vertical velocity fluctuations compared to larger aircraft. Larger aircraft are unable to fly as close to the sea surface and are therefore less suitable for estimating surface fluxes in thin stable boundary layers over the sea. For flight levels closer to sea surface, the flux displacement error is expected to be larger because of larger vertical gradients. Unmanned aircraft may suffer larger platform displacement errors because of larger vertical displacements.

Compared to the aircraft, the buoy errors would be enhanced by stronger gradients at the lower observational levels of the buoy, but are reduced by small magnitudes of the buoy displacement and the

small vertical velocities close to the surface. The displacement flux error for the buoy becomes marginally significant only for large wave heights where it averages a few percent.

Using eddy correlation data collected by LongEZ flights perpendicular to the coast, the adjustment of atmospheric flow downstream from a coastline is examined. Along-shore variation of the turbulence over the water is generated by the varying width of the upstream land strip between the sea and inland water. Over the coastal zone, the turbulence is strongest downstream from the widest part of land. The along-shore variation of the turbulence decreases with increasing sea fetch due to horizontal mixing. In other terms, the footprint of the flux farther offshore includes a larger width of upstream land. Beyond 5 km sea fetch, the along-shore variation becomes small.

LongEZ flights perpendicular to the western edge of the Gulf Stream were also studied. With flow of warm air over cooler water, relatively strong intermittent bursts of downward transport of momentum occur above the surface inversion over the cooler water. As a result, the magnitude of the spatially-averaged downward momentum flux increases with height, although flux sampling errors are large. With modest increases of surface temperature, significant turbulence and momentum flux sometimes develop even if the airflow remains stable and the heat flux is small upward or downward. Apparently, the reduced stratification allows development of significant shear-generation of turbulence. Here, the increase of surface temperature in the downwind direction acts more as a catalyst for shear generation of turbulence in contrast to the convective internal boundary layer where direct buoyancy generation of turbulence dominates. More substantial increases of surface temperature, as occurs at the main SST front, lead to significant buoyancy-generation of turbulence and warming of the air downwind from the surface front. The resulting horizontal temperature gradient contributes to a local hydrostatic pressure gradient, which accelerates flow towards the warmer air.

The triggering of shear-generation of turbulence by modest increases of surface temperature in the flow direction may be much more frequent than the development of convective internal boundary layers downwind from large surface temperature changes, which cause thermal instability. Surface temperature changes over land and sea are often not sufficiently strong to change stable stratification to unstable conditions with upward heat flux.

Internal boundary layer development in offshore flow of warm air over cool water is studied numerically, using a two-demensional high-resolution mesoscale model with a turbulent kinetic energy closure scheme, and a three-dimensional large-eddy simulation model that explicitly resolves the largest turbulent scales. The model is compared with offshore flow in SHOWEX. The decoupling of the weakly-convective boundary layer from the sea surface, as it is advected offshore, and the formation of a stable internal boundary layer, provide a severe test of the turbulence closure scheme. With the existing mixing-length scheme, the model performs poorly. Increasing the mixing-length from that predicted by the existing surface-based formulation, improves the model comparisons with the observations.

PUBLICATIONS

Mahrt, L., D. Vickers, J. Sun, T. Crawford, G. Crescenti, and P. Frederickson, 2001: Surface stress in offshore flow and quasi-frictional decoupling. *J. Geophys. Res.*, **106**, 20,629-20,639.

Mahrt, L., D. Vickers, W. Drennan, H. Graber and T. Crawford, 2003: Fluxes measured from moving platforms. To appear *J. Atm. and Oc. Tech.*

Moore, Erin and L. Mahrt, 2003: Along-shore variations of offshore flow. *Geophys Rev Letters,* **30**, 1109-1113.

Mahrt L., D. Vickers, P. Frederickson, K. Davidson and A.-S. Smedman, 2003: Sea-surface aerodynamic roughness. To appear in *J. Geophys. Res.*

Mahrt, L., D. Vickers and Erin Moore, 2003: Flow adjustments across sea-surface temperature changes. To appear in *Boundary-Layer Meteorol.*

Skyllingstad, E., R.M. Samelson and L. Mahrt, 2003: A numerical modeling study of warm offshore flow over cool water. Submitted to *J. Geophys. Res.*

Surface stress in offshore flow and quasi-frictional decoupling

L. Mahrt,[1] Dean Vickers,[1] Jielun Sun,[2] Timothy L. Crawford,[3] Gennaro Crescenti,[3] and Paul Frederickson[4]

Abstract. Aircraft data collected at approximately 15 m above the sea surface in the coastal zone are analyzed to examine the spatial distribution of surface stress. Advection of stronger turbulence from land dominates the near-surface turbulence for the first few kilometers offshore. With offshore flow of warm air over cold water, strong stratification leads to very small surface stress. Because the stability restricts the momentum transfer to the waves, the aerodynamic surface roughness decreases to very small values, which in turn decreases atmospheric mixing. The redevelopment of the boundary layer farther downstream is examined. Computation of fluxes from observations for stable cases is difficult due to a variety of errors including large random flux errors, possible instrumental loss of small-scale flux, difference between the surface flux and that at the observational level, and inadvertent capture of mesoscale motions in the computed turbulent fluctuations. Although the errors appear to be substantial, the aircraft momentum fluxes compare favorably with those from sonic anemometers on two buoys and a tower at the end of a 570-m pier, even with near collapse of the turbulence.

1. Introduction

Existing models of the air-sea interaction sometimes break down in the near-coastal zone due to advection of stronger turbulence and temperature from land, nonstationarity associated with diurnally varying horizontal pressure gradients in the atmosphere, complex wave states, including young wind-driven waves and incoming swell, and shoaling of such swell. A number of studies have formulated transfer coefficients in terms of fetch [*Perrie and Toulany*, 1990] or wave age [e.g., *Geernaert et al.*, 1987; *Toba and Koga*, 1986; *Maat et al.*, 1991; *Vickers and Mahrt*, 1997a].

Advection of stronger turbulence from land can strongly influence the air-sea interaction in offshore flow [*Mahrt et al.*, 2001; *Vickers et al.*, 2001]. Some of the perceived dependence on wave age in offshore flow, whether based on friction velocity or wind speed, may be due to the influence of advection of stronger turbulence from the land surface, which decays in the downstream direction and influences the drag coefficient in a manner similar to the wave age dependence [*Sun et al.*, 2001]. This advection links the fluxes over the sea with the characteristics of the upstream land surface. *Winstead and Young* [2000] and N. Winstead and P. Mourad (Shallow great lakes scale atmospheric thermal circulation imaged by synthetic aperture radar; submitted to *Monthly Weather Review*, 2001) find that alongshore variation of land characteristics (farmland, woods, and towns) leads to alongshore variation of high-frequency surface wave energy in offshore flow; more wave energy is generated downstream from rougher land surfaces.

With offshore flow of warm air over cool water, the turbulence and surface stress can become suppressed by the stratification, referred to as quasi-frictional decoupling by *Smedman et al.* [1997a, 1997b], perhaps analogous to development of the very stable nocturnal boundary layer over land. Over land, surface cooling and stratification of the air near the surface reduces turbulence and downward heat flux, which leads to stronger net cooling of the surface and further enhancement of the stratification. Over the water the surface temperature is more constant, but the reduction of downward momentum flux by the stratification reduces generation of the surface wave field, which in turn reduces the surface roughness [*Plant et al.*, 1998] and subsequently reduces mechanical generation of atmospheric turbulence. Over land the roughness length is normally considered to be a constant for a given location and wind direction.

The partial collapse of turbulence in offshore flow of warm air over cooler water is emphasized in this study because it is the case most poorly simulated by existing models. On the basis of observations in the coastal zone in the Baltic Sea, *Smedman et al.* [1997b] find that the atmospheric boundary layer over the Baltic Sea is stable more often than unstable and the influence of warm air advection from land can extend 150 km offshore. In this study, offshore flow will be examined in terms of eddy correlation aircraft data collected approximately 15 m above the sea surface (section 3). In the next section we review the basic formulations required for the analysis in sections 4–7, using the data described in section 3.

2. Existing Parameterization of the Surface Stress

The drag coefficient is computed as

$$C_d = \frac{u_*^2}{\overline{U}^2},\qquad(1)$$

where u_* is the friction velocity based on averaged components of the stress vector and U is the wind speed computed from

[1]College of Oceanic and Atmospheric Sciences, Oregon State University, Corvallis, Oregon, USA.
[2]National Center for Atmospheric Research, Boulder, Colorado, USA.
[3]NOAA Air Resources Laboratory, Idaho Falls, Idaho, USA.
[4]Naval Postgraduate School, Monterey, California, USA.

averaged wind components. Given observations of the wind speed and surface stress, the roughness length can be "backed out" of the similarity prediction of the drag coefficient.

$$C_d = \left[\frac{\kappa}{\ln (z/z_o) - \psi_m} \right]^2, \qquad (2)$$

where z is the observational level, z_o is the roughness length for momentum, κ is the von Karmen constant, taken as 0.4, and ψ_m is a function of the stability z/L, where L is the Obukhov length, expressed as

$$L = - \frac{u_*^3}{(\kappa g/\theta_v)([\overline{w'\theta'}] + 0.61\theta[\overline{w'q'}])}, \qquad (3)$$

where θ is the potential temperature and q is the specific humidity. The stability function will be computed from *Paulson* [1970] for unstable conditions and from *Dyer* [1974] for stable conditions.

Using (2), the aerodynamic roughness length z_o can then be estimated from the observed values of u_*, U, and L and the specified function ψ. The computed roughness lengths could include compensation for incorrect stability functions ψ. However, Monin-Obukhov similarity theory was found to be a good approximation for the flux-gradient relationship in quasi-stationary homogeneous flow over the sea in terms of the turbulence energy budget [*Edson and Fairall*, 1998; *Wilczak et al.*, 1999] and flux-gradient relationship [*Vickers and Mahrt*, 1999], although modest adjustments of the stability function were suggested in the later study. The dependence of the roughness length on stability is equivalent to a dependence of the neutral drag coefficient on stability. Often the drag coefficient is reduced to a neutral value to remove the influence of stability. The neutral drag coefficient may exhibit a dependence on stability, which is sometimes interpreted as failure of Monin-Obukhov similarity theory or a failure of the existing stability functions. However, the reduction of the drag coefficient to neutral conditions assumes either constant roughness length or the Charnock formulation [*Charnock*, 1955] with constant coefficient. Both assumptions may be incorrect and are not a part of Monin-Obukhov similarity theory. Therefore a stability-dependent roughness length is not necessarily an indicator of the failure of Monin-Obukhov similarity theory.

3. Data and Analysis

Surface fluxes are estimated for the Shoaling Waves Experiment (SHOWEX) in October–November 1997 and March 1999 and in November–December 1999 [*Sun et al.*, 2001; *Crescenti et al.*, 1999; *French et al.*, 2000] using the low-level aircraft data from 37 flights on 35 days at an average height 15 m above the sea surface. The data were collected by the LongEZ research aircraft over Atlantic coastal water off the Outer Banks near Duck, North Carolina. The SHOWEX data have minimal instrumentation problems compared with the previous two field programs and several improvements in preprocessing and will be emphasized in this study.

For both experiments in 1999, a Campbell CSAT sonic anemometer (10-cm path length) operated at approximately 18 m above the water on a tower at the end of a 570-m pier (U.S. Army Corps of Engineers Field Research Facility). In November–December 1999 a second CSAT sonic anemometer was deployed on a 3-m boom attached to the top of the railing at the end of the pier, 8 m above the sea surface. To avoid serious

flow distortion, we include only those time periods with winds from the northerly sector between 295 and 70 degrees for the northward pointing sonic anemometer on the rail, and easterly flow between 360 and 180 degrees for the eastward pointing 18-m sonic on the tower. Smoke releases indicated that the distortion due to the pier for the accepted wind directions did not extend to the end of the 3-m boom, which is consistent with the close agreement between the fluxes computed from the 18- and 8-m sonic anemometers. Both the aircraft and sonic anemometer data were subjected to quality control procedures similar to those described by *Vickers and Mahrt* [1997b].

3.1. Flight Pattern and Analysis Strategy

Thirteen flights from the three experiments measured horizontal and vertical structure in the lowest few hundred meters above the sea surface in the first 10–20 km offshore. Other types of flight patterns include a series of flight tracks parallel to the shore, box patterns, 100-km transects perpendicular to the coast, and a few mission-specific patterns. For the analyses in sections 4–7, all flights are used that collected low-level data over the Atlantic side of the Outer Banks with a fetch greater than 10 km for offshore flow.

3.2. Vertical Flux Divergence

Smedman et al. [1997a, 1997b] point out that the boundary layer may be very thin in stable conditions over the sea and that standard observational levels may be too high to estimate surface fluxes. Even though the LongEZ generally flew about 15 m above the sea surface, the difference between the flux at this level and the sea surface stress may be significant in thin boundary layers or advective conditions. The difference between the stress at the aircraft level and the sea surface is constrained by the equation of motion. Integrating the equation of motion for the offshore flow component between the surface and the aircraft level, z, for stationary flow, the surface stress is

$$\overline{w'u'}_{sfc} = \overline{w'u'}_z - \int_{sfc}^{z} \left[\bar{u} \frac{\partial \bar{u}}{\partial x} + \bar{w} \frac{\partial \bar{u}}{\partial z} + \frac{\partial \overline{u'^2}}{\partial x} \right] dz + \int_{sfc}^{z} f(\bar{v}$$

$$- V_G)\, dz, \qquad (4)$$

where we have neglected derivatives parallel to the coast (here the y direction), f is the Coriolis parameter, and V_G is the geostrophic wind. The difference between the momentum flux at the sea surface and at the observational level $z \approx 15$ m is constrained by the magnitude of the advection, horizontal flux divergence, and the ageostrophic term (the last term on the right-hand side).

Vickers et al. [2001] find that within the first few kilometers downstream from the coast, strong horizontal advection of weaker momentum is partially balanced by vertical convergence of the downward turbulent momentum flux and downward advection of stronger momentum by mean subsidence. The subsidence is associated with acceleration of offshore flow. On the basis of x-z cross-section analysis of the stress in stable offshore flow using multiple aircraft levels, *Vickers et al.* [2001] found the surface stress to be typically of the order of 10^{-2} m^2 s^{-2} smaller than the stress at the 15-m aircraft level in the first few kilometers of offshore flow. This difference can be more than 30% of the absolute flux value.

Farther offshore, advection terms become small but the depth of the turbulence might be very thin (section 6). Then

the stress divergence between the aircraft level and the surface is supported by the large-scale ageostrophic flow $f(\bar{v} - V_G)$, which is expected to be of the order of 10^{-4} m s^{-2}. This value corresponds to a change of stress of 1.5×10^{-3} m^2 s^{-2} between the surface and the aircraft level. This value is only a little smaller than the smallest stress values observed in stable offshore flow (section 4) and therefore could be important. That is, the stress at 15 m might be significantly smaller than that at the sea surface.

The influence of the height of the platform on the computed roughness length will be an important concern in this study. The height of the aircraft for low-level flights included here ranged from roughly 10 m to a specified upper cutoff of 20 m. Roughness lengths computed from the aircraft data within this range of heights do not show a clear dependence on the height of the aircraft. Comparison of the two levels of momentum and heat flux measurements at the end of the pier for onshore flow shows good agreement. However, the computed roughness length is systematically smaller at the 18-m level. This appears to be due to the increase of wind speed with height faster than predicted by similarity theory. Perhaps the 18-m level is often above the surface layer, which would also imply that the aircraft was sometimes above the surface layer.
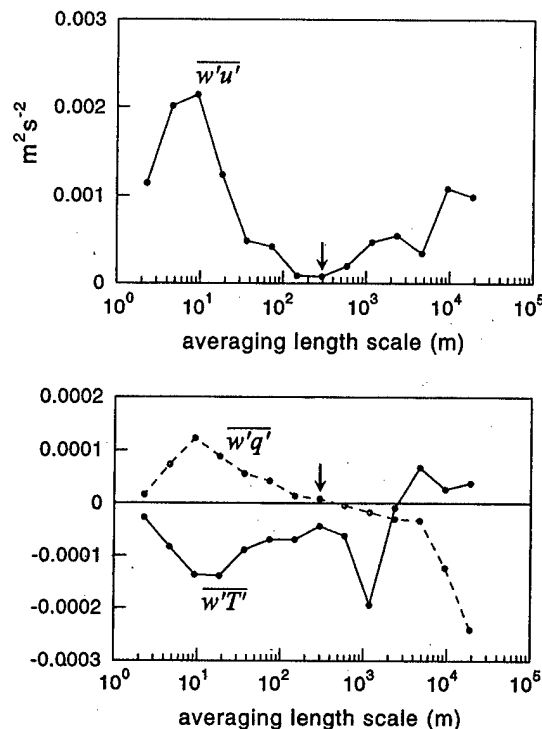
3.3. Variable Averaging Length

In this study the dependence of the fluxes on averaging scale is studied in terms of multiresolution cospectra [e.g., *Howell and Mahrt*, 1997], which can be thought of as a wavelet decomposition using unweighted averaging lengths of different (dyadic) lengths as the local basis set. Interpretation of such cospectra does not require the assumption of periodicity, and the properly integrated multiresolution cospectra exactly satisfy Reynolds averaging.

For very stable conditions, fluxes can be quite small and confined to small horizontal scales, less than 100 m. As a result, the usual use of a 1-km window may capture significant nonturbulent mesoscale flux, which can be primarily flux sampling errors. Normally, this mesoscale flux is small compared with the turbulent flux. However, with very stable conditions, the turbulent flux is small, and the mesoscale scale flux may even dominate the computed flux. Therefore we have used a smaller averaging window to define perturbations for very stable conditions. The averaging length is determined separately for each 5-km record based on an empirical relationship (constructed below) between the averaging length and the bulk Richardson number,

$$Rb = \frac{g}{\theta} \frac{\delta\theta z}{\overline{U}^2}, \tag{5}$$

where $\delta\theta$ is the difference of potential temperature between the aircraft level and the sea surface. The bulk Richardson number is used instead of z/L, since the later is a stronger function of the averaging length itself. The sea surface temperature measured from the LongEZ was calibrated using buoy measurements for each flight day.

The length scale associated with the gap region separating turbulence and mesoscale transport is estimated from cospectra of momentum, heat, and moisture for individual flights (Figure 1). A gap scale was identified when the slope of the cospectra changed sign or when the cospectra crossed zero for length scales exceeding an arbitrary threshold of 100 m. For most flights the gap scales identified for each of the three

Figure 1. Determination of the averaging length based on the cospectral gap or cospectral sign reversal (vertical arrow) for (a) momentum flux (m^2 s^{-2}), and (b) heat flux (m s^{-1} °C) (solid line) and moisture flux (m s^{-1} g kg^{-1}) (dashed line) in stable conditions for a single aircraft pass on November 21.

cospectra were approximately equal. When the gap scales for the momentum, heat, and moisture fluxes were not the same, we chose an average value even though the gap scale often seemed better defined for moisture where the cospectra typically changed sign in the gap region (cospectral zero crossing).

The values of the gap scale, averaged for different intervals of Rb (Figure 2), were fit to a simple model where horizontal length scale decreases from near 5 km for unstable conditions to only 100 m for very stable conditions (Figure 2). The fluxes based on deviations from the stability-dependent averaging
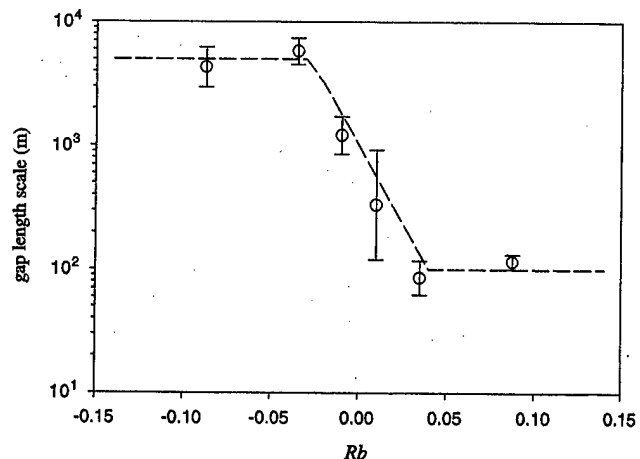
Figure 2. Dependence of the flux averaging length on the bulk Richardson number for bin-averaged values (circles) with the standard error indicated by vertical brackets, and the simplified model fit (dashed line).

length are then averaged over 5-km segments to reduce random flux errors. Application of the variable averaging length tends to increase the fluxes in unstable conditions, on average, and decrease fluxes in stable conditions, on average. However, this systematic change is small, and application of the variable averaging length does not influence the qualitative conclusions of sections 4–7. The most significant change is a reduction of heat flux for stable conditions; however, this changes the log of the roughness length by less than 10%, on average.

3.4. Other Flux Computation Problems

The aircraft data were collected at 50 samples s^{-1} with an air speed of about 55 m s^{-1}, corresponding to a sample interval of about 1 m. Fluxes on horizontal scales smaller than 2 m are lost. This small-scale flux is expected to be missing since the data were low-pass filtered to remove noise at smaller scales. As a result, there is no folding back of small-scale flux to lower frequencies via aliasing. In semicollapsed situations the cospectra do not decrease to small values at the smallest resolvable scale of about 2 m. This implies that momentum flux occurs at even smaller scales. In fact, in a few cases, the cospectra appeared to peak at scales less than 10 m!

As a measure of potential flux loss, we examined the ratio of the flux at the smallest dyadic scale of the multiresolution cospectra to the total flux. With no small-scale flux loss, this ratio should be small. For the momentum flux this ratio increases with stability as the transporting eddies shift to smaller scales, averaging 10% for very stable conditions.

In addition, significant heat flux may be lost for very stable conditions due to the response time of the thermistor, which corresponds to a horizontal scale of 3–4 m. The cospectra of the heat flux tends to vanish at the smallest resolvable scale because the sensor could not resolve variations on this scale. Greater heat flux loss compared with the momentum flux loss causes the estimated stability z/L to be too small. For stable conditions this error acts to underestimate the stability function and therefore to underestimate the roughness length computed from (2). In subsequent sections we use fluxes where no attempt was made to correct for small-scale flux loss, which is under further investigation.

Fluctuations of the aircraft height above the surface, typically of the order of a few meters on a horizontal scale of a kilometer, lead to artificial fluctuations in the presence of mean vertical gradients. The corresponding error for the momentum flux is normally small for unstable conditions. It is large for individual stable records but is not systematic (it occurs with either sign with equal probability) except for very stable conditions, where it acts to overestimate the momentum flux, on average, by 40–50%. The corresponding error in the heat flux is very small. The net effect is to underestimate z/L and the aerodynamic roughness length. Analysis of such errors is complicated and will be reported on in a future paper. Finally, the aircraft may overestimate the wind speed in weak wind conditions, causing the drag coefficient and roughness length to be underestimated.

While the above flux uncertainties seem complex and serious, the aircraft fluxes did compare well with one week of fluxes acquired by the Naval Postgraduate School flux buoy located 10.5 km off the coast (Duck) in 23 m of water (see Figure 5, section 5.1). The LongEZ flew four flights over the buoy during the first week of March 1999. The fluxes from the LongEZ and buoy agreed within the random flux error. On March 2 and 4 the surface friction velocity was small, approximately 0.1 m s^{-1} for both platforms. Stress values from the aircraft data also agree reasonably well with measurements from sonic anemometers mounted on buoys and a sonic anemometer on an offshore tower during SHOWEX (section 5.1). Agreement between instruments does not necessarily imply accurate fluxes since all of the above platforms may underestimate the flux in stable conditions.

Computation of the roughness lengths using Monin-Obukhov similarity theory may be inapplicable if the stress does not approximately oppose the wind. The stress direction may be altered by swell. The influence of swell for weak wind conditions [Smedman et al., 1999; Grachev and Fairall, 2001] can cause upward momentum flux from the wave field to the atmosphere, in which case the aerodynamic roughness length has no meaning. In the subsequent analyses we eliminate data where the stress direction deviated by more than 45 degrees from the vector opposite the wind direction. This condition leads to a reduction of the averaged roughness length for weak wind speeds (section 7).

4. Near-Coastal Zone

To organize the discussion, we define three offshore zones for the flow of warm air over cold water: The first is the near-coastal zone, where the stress and roughness length decrease rapidly with fetch in the first few kilometers offshore for stable conditions (Figure 3, solid lines); the second is the quasi-frictional decoupling zone (section 5), where the stress and roughness length maintain extremely small values, often for more than 20 km offshore; the third is the recovery zone, where the stress and roughness length increase, sometimes abruptly (section 6).

Vickers et al. [2001] found that in the first few kilometers offshore, vertical convergence of the downward momentum flux acts to accelerate the flow in the downstream direction. At a fixed point the flow is relatively stationary. The vertical transport of turbulence energy for short fetch is also downward (Figure 4). This downward transport contrasts with the normal concept of a boundary layer, where the vertical transport of turbulence energy is either upward or small. Here this downward transport of turbulence is expressed in terms of the vertical velocity variance since the horizontal velocity variances are more sensitive to choice of averaging length. The vertical transport of the vertical velocity variance ($\overline{w'^3}$) is upward for all of the unstable cases and significantly downward for four of the seven stable cases.

Downstream from the coast the roughness length is expected to increase with wave age (C_p/u_*) with very young wind-driven waves due to increasing amplitude of the waves, until a wave age of 5–10 [e.g., Nordeng, 1991], where C_p is the phase speed of the dominant wave. As the wave age increases further, the roughness length decreases due to increasing phase speed of the wind-driven waves and reduction of the relative flow over the waves. The initial stage of increasing stress with increasing fetch, due to wave initiation, is not observed in our data because of the greater influence of advection of turbulence from land [Sun et al., 2001]. Beyond this conclusion, effects of wave state and advection of stronger turbulence from land are difficult to isolate. The advection of stronger turbulence from land can lead to greater downward transport of momentum over the sea, which presumably enhances wave growth, just downstream from the coast.
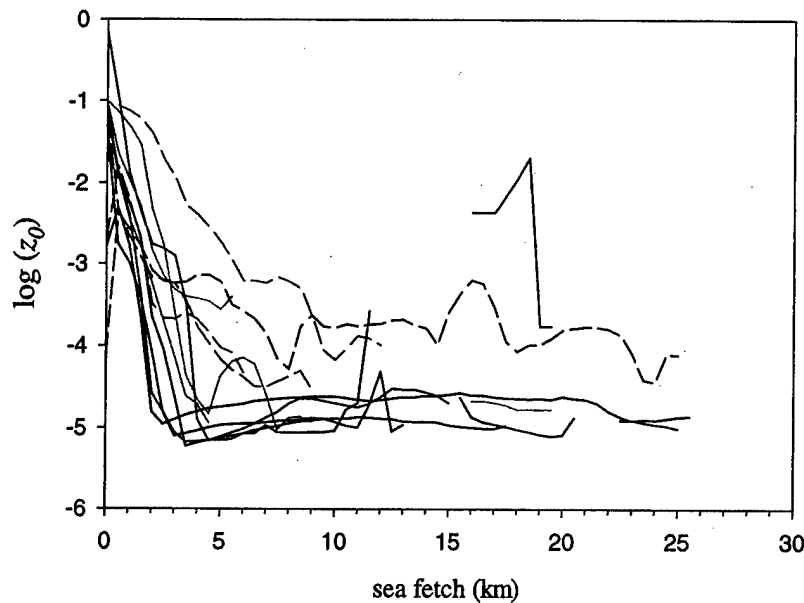
Figure 3. The roughness length as a function of fetch based on heat and momentum fluxes extracted from the 10-m level of the cross-section analyses (section 3.1) for unstable (broken lines) and stable (solid lines) conditions. To remove some extremely small values of roughness lengths and restrict the vertical range of the plot, the roughness length is not allowed to decrease below the smooth flow value (for this plot only). This condition accounts for leveling off of the roughness length in stable cases beyond a fetch of a few kilometers.

5. Quasi-frictional Decoupling Zone

In flow of warm air over cooler water, the stress, turbulence energy, and roughness length decrease by orders of magnitude in the first few kilometers offshore (Figure 3), as opposed to near-neutral and unstable conditions, where they decrease much more slowly. Therefore the stability over the water affects the rate of decrease of the turbulence downstream from the coast. The reduction of downward momentum transfer by the atmospheric stability restricts wave generation and causes very small surface roughness lengths (Figure 3), as previously noted by Plant et al. [1998]. These very small surface roughness lengths, in turn, lead to weaker turbulent mixing, and so forth. With such "quasi-frictional decoupling" [Smedman et al., 1997b], the observed aerodynamic roughness length decreases to values several orders of magnitude smaller than the smooth flow value, as also found here. In this study we will loosely refer to quasi-frictional decoupling as cases where the computed roughness length becomes comparable to or substantially less than the smooth flow value. While we recognize that the roughness length may be significantly underestimated (section 3), these conditions correspond to very weak turbulence and values of the friction velocity significantly less than 0.1 m s^{-1}.
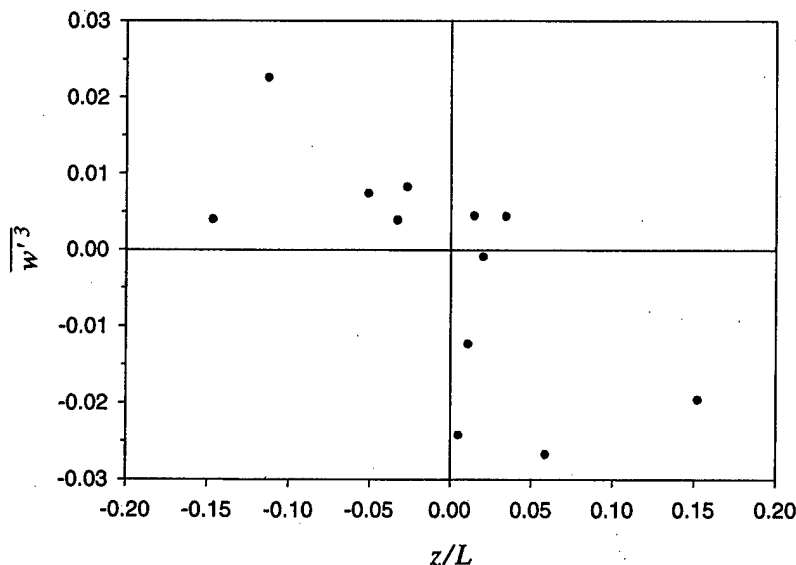
Figure 4. The vertical transport of vertical velocity variance, averaged over the first 2 km offshore as a function of stability.
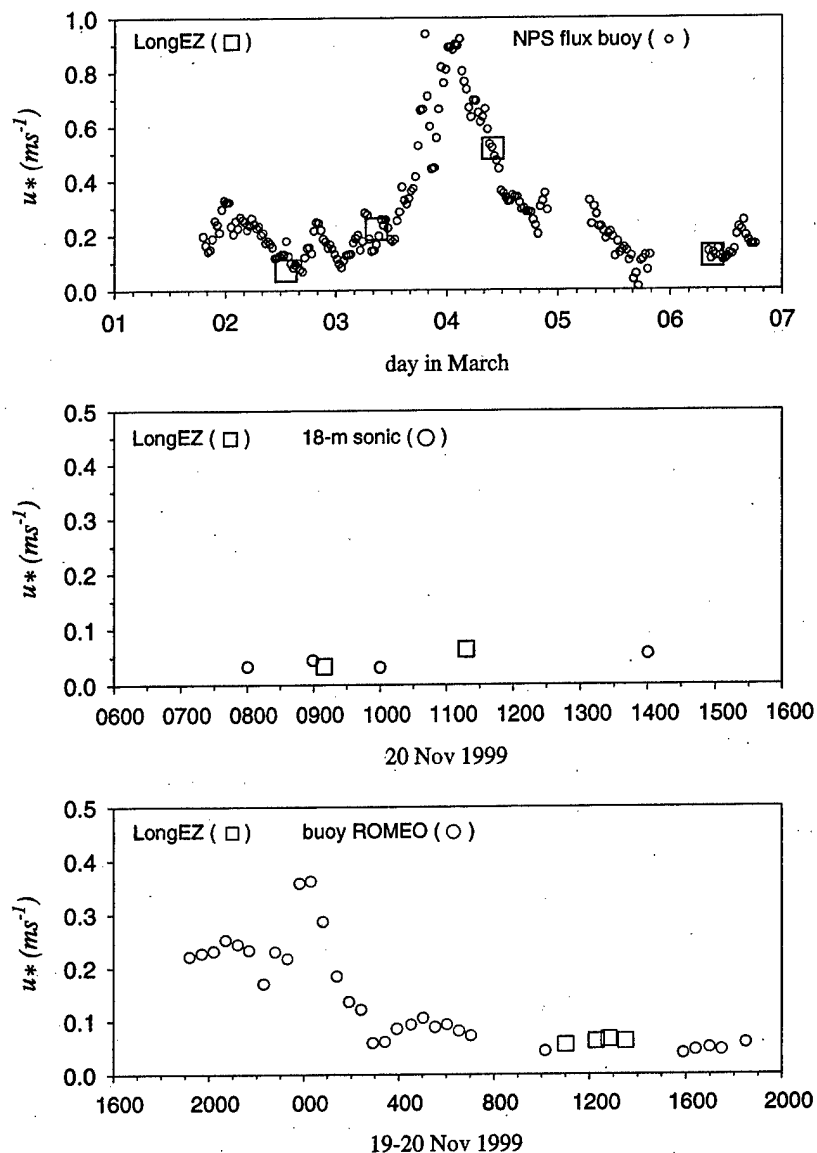
Figure 5. (a) Comparison between the friction velocity for the LongEZ and the Naval Postgraduate School buoy for the period of overlapping observations in March 1999, (b) comparison between the LongEZ friction velocity and that for the 18-m sonic anemometer on November 20, 1999, and (c) comparison between the LongEZ friction velocity and that for buoy Romeo on November 20, 1999.

These small values imply that the flow at the observational level is not fully coupled to the surface in the sense of the usual atmospheric boundary layer.

Here the quasi-frictional decoupling at the observational level begins with travel times typically of the order of 10 min, generally corresponding to fetches greater than 3–5 km (Figure 3), depending on wind speed and upstream turbulence over the land. Even though z/L is significant positive, the buoyancy flux can be relatively small because u_* is small.

5.1. Ultrasmooth

Donelan [1990, p. 265] also calls attention to extremely small roughness lengths referred to as "ultrasmooth" conditions. Variations of surface tension and only small differences between the dominant wave phase speed and wind speed were cited as possible causes. The latter does not appear to be the cause near the coast in this study, where the wind-driven waves

are young and the swell opposes the offshore flow. It must be remembered that the aerodynamic roughness length is computed using the stability functions (section 2) and as such does not necessarily have a definable relation to wave state. In other terms, ultrasmooth values of the aerodynamic roughness length do not necessarily imply glassy seas.

While observational errors are large for cases of weak fluxes (section 3), sonic anemometer data show a similar semicollapse of the turbulence. Sonic anemometer measurements at the end of the 570-m pier can be used only with onshore flow where the influence of flow distortion from the tower and the pier is minimized. On November 20, 1999, the flow was weak onshore, with a stable air-sea temperature differences of about 1°C. On this day the friction velocity from the tower (Figure 5b), the buoy Romeo (Figure 5c) (provided by W. Drennen), and the aircraft all show small friction velocity values of approximately 0.05 m s^{-1}. Good agreement is also shown be-
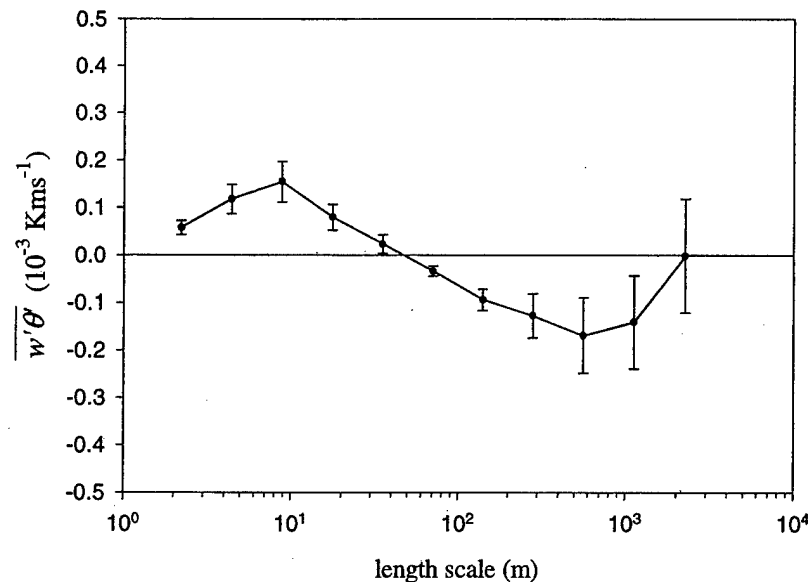
Figure 6. Kinematic heat flux as a function of horizontal scale composited for the seven passes for November 20, 1999. The vertical brackets indicate the standard error based on the between-pass variability for the seven passes.

tween the LongEZ friction velocity and that from the Naval Postgraduate School buoy [*Frederickson and Davidson*, 2000] for the overlap period in March of 1999 (Figure 5a), including a semicollapsed period. We conclude that the surface stress is extremely small but cannot categorically conclude ultrasmooth conditions because of potentially significant flux errors.

The cospectra on this day systematically show upward heat flux at horizontal scales smaller than 50 m and downward heat flux at larger scales (Figure 6). Apparently, the initial overturning corresponds to downward heat flux which destabilizes the flow (cold air on top of warm air). This destabilization leads to upward heat flux by smaller-scale eddies. *Piccirillo and Van Atta* [1997] also find upward buoyancy flux on smaller scales and downward buoyancy flux on larger scales in a stratified wind tunnel with shear. This small-scale upward heat flux was not a systematic condition for stable conditions in SHOWEX.

5.2. Minimum Wind Speed

With offshore flow of air several degrees warmer than the sea surface temperature, ultrasmooth roughness lengths are computed from the present data even for 15-m wind speeds exceeding 10 m s^{-1}. For example, on March 18, 1999, the wind speed reached 12 m s^{-1} while the friction velocity and standard deviation of the vertical velocity both fell below 0.1 m s^{-1}, corresponding to values of the roughness length smaller than the smooth flow value.

This finding for very stable conditions contrasts with the literature where the minimum wind speed for generation of surface waves is considered to be much smaller. The smooth flow regime is often thought to occur, on average, when the wind speed is less than 2.8 m s^{-1} [*Kitaigorodski and Donelan*, 1984] although smooth flow viscous effects can be important up to wind speeds of about 7.5 m s^{-1}. *Kahma and Donelan* [1987] report a range of minimum wind speeds between 0.4 and 5.5 m s^{-1} for initiation of capillary-gravity waves in a laboratory environment. On the basis of radar backscatter, the minimum wind speed for generation of surface waves is esti-

mated to be in the range from 1.0 to 2.0 m s^{-1} [*Moller et al.*, 2000; *Plant et al.*, 1999], although a variety of observational errors for weak wind conditions have been noted [*Moller et al.*, 2000; *Freilich and Dunbar*, 1999; *Weissmann and Graber*, 1999].

6. Recovery Zone

Theoretically, one might expect slow recovery from quasi-frictional decoupling, induced by gradual development of the wave field responding to the weak surface stress, and gradual reduction of the stratification near the surface as the air-sea temperature difference decreases downstream. However, in practice, spatial variation of the sea surface temperature and wind field seem to be more important on a given day, and the recovery from quasi-frictional decoupling seems to assume a different form for each available case. The recovery can take the form of a sudden redevelopment of turbulence, and the turbulence may collapse again farther downwind. However, for most of the cases, the turbulence did not recover within the observational domain, typically extending to 10–20 km from the coast.

For example, the roughness length is still at the smooth flow value, or smaller, at 20-km fetch for four of the five cases of offshore stable flow with complete data coverage out to 20 km (Figure 3). The fifth case, on March 6, 1999, indicates rapid enhancement of the roughness length at 15–20 km offshore. This recovery to large roughness lengths is characterized by downward transport of turbulence energy from higher levels. The latter suggests that the turbulence originates from instability above the thin, cool marine layer and then is transported downward toward the surface. Perhaps the generation of this turbulence is associated with the acceleration of the decoupled flow and enhanced shear above the thin, cool marine layer.

Only limited information is available on the vertical structure in the recovery zone. On November 3, 1997, the flight plan was devoted to sampling the vertical structure of the boundary layer through numerous slant soundings from the coast out to 100 km. On this day the flow was offshore and slightly warmer
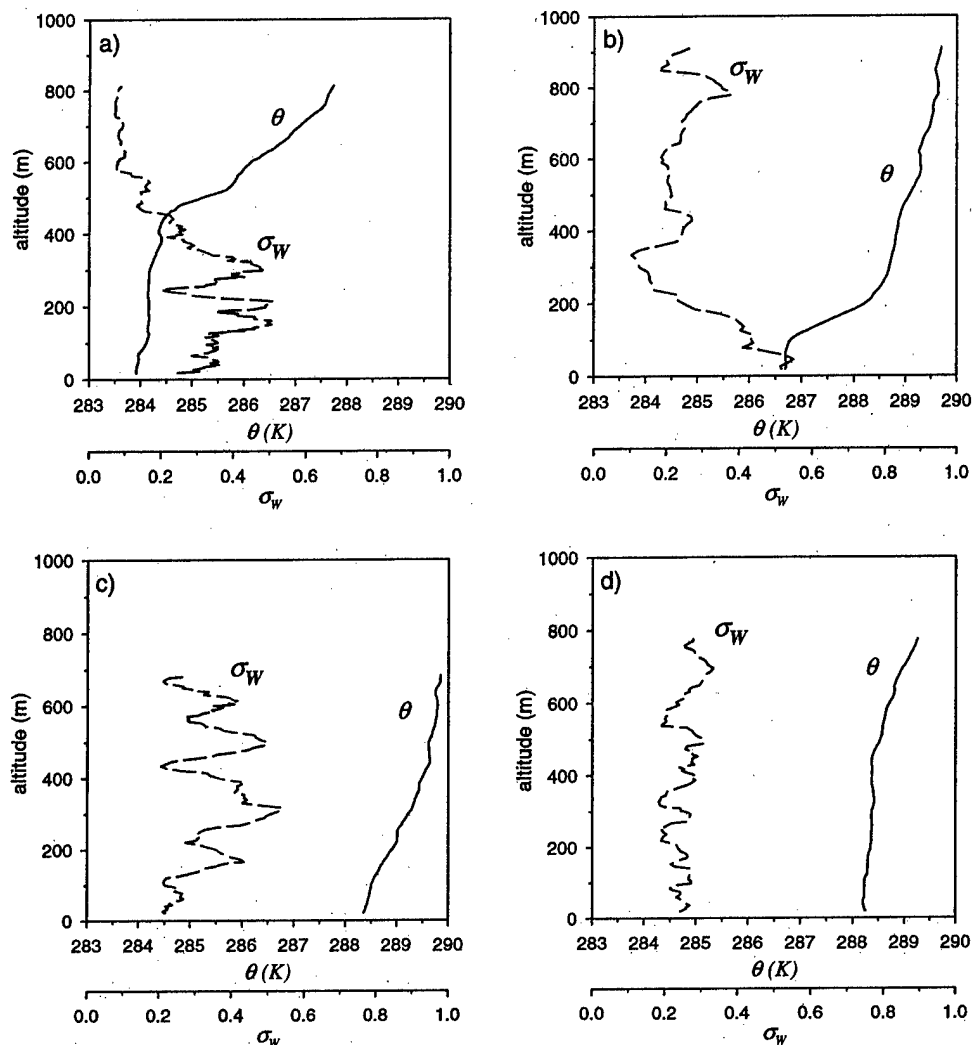
Figure 7. Example slant aircraft soundings of potential temperature and the standard deviation of vertical velocity for November 3, 1997.

than the sea surface. The standard deviation of vertical velocity constructed from slant soundings is noisy because of inadequate sampling at a given level and because of contamination of the computed perturbations by variations of the mean flow within the averaging window of 1 km, as the aircraft ascends and descends. Such errors artificially prevent the standard deviation of vertical velocity from reaching very small values. With a typical ascent rate of 2%, the 1-km averaging length corresponds to a vertical elevation change of 20 m. The sequential soundings indicate a variety of boundary layer structures, and the boundary layer is sometimes poorly defined. The thin, cool boundary layer is observed in only some of the soundings and in other cases may be confined to below the lowest observation level of about 30 m. A few examples are included in Figure 7. Figure 7a shows a deep 400-m boundary layer, while Figure 7b shows a thinner, well-defined boundary layer with significant turbulence over a depth of 100 m. Figure 7d might correspond to a deep boundary layer, while the boundary layer cannot be readily defined in Figure 7c.

Surprisingly, the vertical structure did not seem to vary systematically with offshore distance, suggesting more than one collapse and recovery sequence. The stability on this day is substantially weaker than that for the ultrasmooth case on March 6, 1999, discussed above. The sequential soundings indicate that individual soundings on this day would be misleading and that the evolution and elimination of the stable internal boundary layer may be intermittent. As one possible explanation, accelerating flow above the thin, cool stable layer enhances the shear and induces mixing (boundary-layer recovery), which in turn reduces the shear and increases the Richardson number. This would lead to decay of turbulence and reformation of the cool stable layer adjacent to the surface. Unsteadiness of the upstream wind may also be a factor, particularly since the fetch at a given point is sensitive to wind direction.

7. Roughness Length Dependence on Stability

The aerodynamic roughness length generally decreases with increasing bulk Richardson number except for the most stable conditions (Figure 8). For the calculations in Figures 8 and 9, a lower threshold of 10^{-10} m was imposed on the roughness length to restrict the range of the vertical axis. Roughness lengths this small are probably zero within observational error. Therefore mean values in Figures 8 and 9 approaching 10^{-10} m
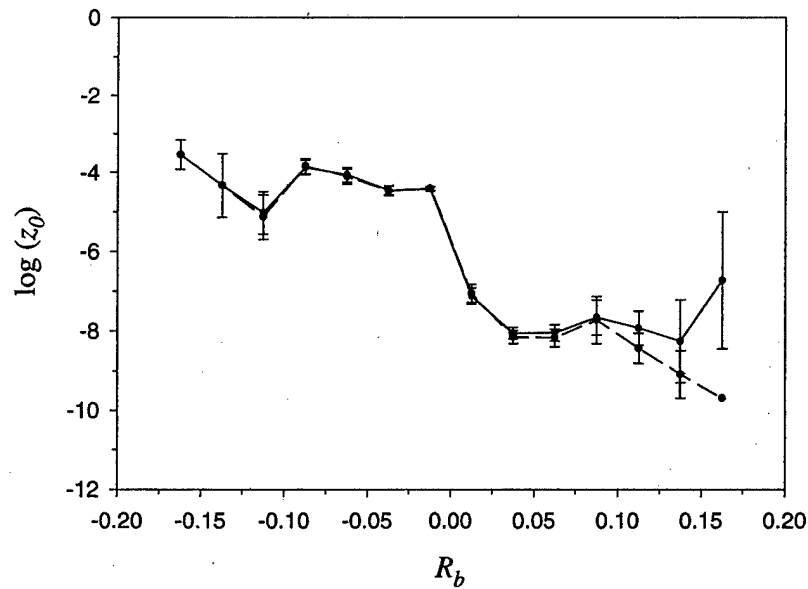
Figure 8. The dependence of the aerodynamic roughness length on the bulk Richardson number for November–December 1999 (solid line) and after removing cases with downward transport of vertical velocity variance (dashed line). Vertical brackets indicate the standard error.

imply that the roughness length is zero within observational error for many of the cases comprising the average.

Large values of the roughness length for very stable conditions occasionally occur with downward transport of vertical velocity variance toward the surface. Removal of these cases reduces the averaged value of the roughness length for very stable conditions, in which case the roughness length decreases with increasing stability. Since the turbulence in cases of downward transport of turbulence energy is not completely controlled by surface fluxes and z/L, Monin-Obukhov similarity theory may not apply. Then the aerodynamic roughness loses its physical meaning.

The roughness length (and the neutral drag coefficient) reaches a minimum value around 5 m s^{-1} (Figure 9), as is observed in numerous previous studies. This minimum value is thought to occur because of the combination of increasing roughness with increasing wind speed and special effects at weak winds. The special effects for weak winds include the role of surface tension and surfactants, transport by boundary-layer scale convective eddies, and "wave-induced" stress associated with swell.

We require that the stress vector be directed within 45 degrees of opposing the wind vector (section 3) to reduce the contribution of the swell to the composited roughness length.
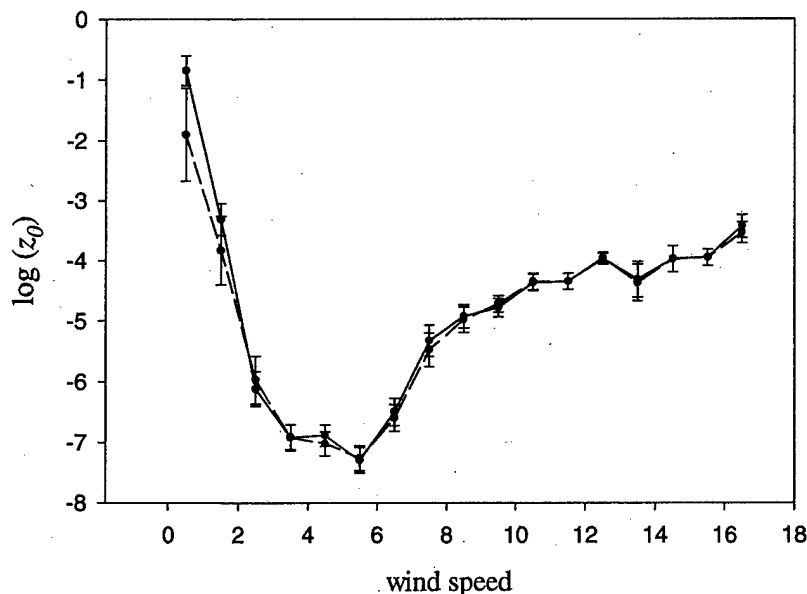
Figure 9. The dependence of the roughness length on wind speed for the November–December 1999 LongEZ data (dashed) and after removing restrictions on the stress direction (section 3) (solid). Vertical brackets indicate the standard error.

Relaxing this criteria (Figure 9, solid line) modestly increases the roughness length (and drag coefficient) at weak wind speeds but has little effect at other wind speeds. Therefore it is likely that part of the increase of the roughness length at weak wind speeds is due to wave-driven stress. The wave-driven stress is not expected to obey Monin-Obukhov similarity theory but enhances the stress and therefore the aerodynamic roughness length computed from that stress.

For weak wind stable conditions, longer waves exert an important influence on the stress, as was observed by *Plant et al.* [1999]. In fact, in their case the stress was nearly constant as the wind decreased to values below a few meters per second. *Rieder and Smith* [1998] find that the wave-induced part of the stress does not vanish as the wind vanishes, causing the drag coefficient to become large. However, they also find that even after attempting to remove the wave-driven stress, some increase of the drag coefficient at weak winds remains. *Mahrt et al.* [1996] found that the increase of the drag coefficient at weak wind speeds over the water is very sensitive to the method of calculation. *Mahrt et al.* [2001] show that the roughness length increases at weak winds speeds also over land surfaces, even over bare ground, alluding to meandering of the wind and stress vectors as a contributing factor.

These weak wind effects contribute to the dependence of the roughness length on stability since the stability tends to increase with decreasing wind speed. However, the present analysis (Figure 9) indicates that the roughness lengths are smallest for a combination of stable conditions and wind speeds in the range of 3-5 m s^{-1}. For winds greater than 6 m s^{-1}, the roughness length increases with increasing wind speed. This increase is due to near-neutral and unstable cases. The roughness length does not increase with wind speed for stable conditions.

8. Conclusions

The above analysis of LongEZ aircraft data and sonic anemometer data reveals frequent occurrence of very small surface stress and roughness lengths. These very small roughness lengths with near collapse of the turbulence are generally associated with advection of warmer air from land over colder water. Numerical estimates of the aerodynamic roughness length may be subject to large errors for weak surface fluxes in very thin boundary layers (section 3) because of significant random flux errors, systematic small-scale flux loss, errors due to fluctuations of the aircraft altitude, and errors in the estimated wind speed by the aircraft. With very thin, stable boundary layers, the stress may decrease significantly between the surface and the observational level. In this case, Monin-Obukhov similarity theory does not apply at the observation level, and the roughness length computed from the data must compensate for this inapplicability. Here "quasi-frictional decoupling" refers to very small values of the surface stress and roughness length and/or extremely thin atmospheric boundary layers. In spite of the above observational difficulties, the small values of the momentum flux inferred from the aircraft data also occur with sonic anemometer data collected from buoys and a tower at the end of a 570-m pier. Ultrasmooth values of the aerodynamic roughness length do not necessarily imply specific information on the wave state. The value of the aerodynamic roughness length only provides the correct flux given the specified stability functions (section 2), and its relationship to wave state in these cases is uncertain [*Sun et al.*, 2001].

The influence of warm air advection extends the influence of land off the coast for tens of kilometers or more. The very small roughness lengths for stable conditions are partly due to reduction of the downward momentum flux by the stable stratification. The data also show the usual minimum of the roughness length and neutral drag coefficient for wind speeds of about 5 m s^{-1}. The larger values of the roughness length at weaker wind speeds are partly associated with large deviations of the stress direction from opposite the wind vector, apparently due to the influence of swell. The very small roughness lengths are most likely to occur with a combination of intermediate wind speeds and stable stratification. Significant wind speed is required here to maintain the advection of warmer air over the cooler sea.

In some stable cases the vertical transport of turbulence may be downward, implying that the main source of turbulence is above the surface-based stable layer. In these cases the aerodynamic roughness length is much larger than that for the usual case of upward transport of turbulence energy. The multitude of physical influences on the surface stress and the difficulty of measuring weak momentum fluxes prevent categorical conclusions.

References

Charnock, H., Wind stress over a water surface, *Q. J. R. Meteorol. Soc.*, *81*, 639–640, 1955.

Crescenti, G. H., T. L. Crawford, and E. J. Dumes, Data report: Long EZ(N3R) participation in the 1999 Shooling Waves Experiment (SHOWEX) pilot study, *Tech. Memo. ERL ARL-232*, Natl. Oceanic and Atmos. Admin., Silver Spring, Md., 1999.

Donelan, M. A., Air-sea interaction, in *Ocean Engineering Science*, edited by B. LeMehaute and D. M. Hanes, pp. 239–292, John Wiley, New York, 1990.

Dyer, A. J., A review of flux-profile relationships, *Boundary Layer Meteorol.*, *7*, 363–372, 1974.

Edson, J., and C. W. Fairall, Similarity relationships in the marine atmospheric surface layer for terms in the TKE and scalar variance budgets, *J. Atmos. Sci.*, *55*, 2311–2328, 1998.

Frederickson, P. A., and K. L. Davidson, Air-sea flux measurements from a buoy in a coastal ocean region, in *Fourteenth Symposium on Boundary Layers and Turbulence*, pp. 530–533, Am. Meteorol. Soc., Boston, Mass., 2000.

Freilich, M., and R. Dunbar, The accuracy of the NSCAT 1 vector winds: Comparisons with National Data Buoy Center buoys, *J. Geophys. Res.*, *104*, 11,231–11,246, 1999.

French, J. R., G. H. Crescenti, T. L. Crawford, and E. J. Dumas, Long EZ participation in the 1999 Shooling Waves Experiment (SHOWEX), *Data Rep. OAR ARL-20*, Natl. Oceanic and Atmos. Admin., Silver Spring, Md., 2000.

Geernaert, G. L., S. E. Larsen, and F. Hansen, Measurements of the wind stress, heat flux, and turbulence intensity during storm conditions over the North Sea, *J. Geophys. Res.*, *92*, 127–139, 1987.

Grachev, A., and C. Fairall, Upward momentum transfer in the marine boundary layer, *J. Phys. Oceanogr.*, *31*, 1698–1711, 2001.

Howell, J., and L. Mahrt, Multiresolution flux decomposition, *Boundary Layer Meteorol.*, *83*, 117–137, 1997.

Kahma, K., and M. Donelan, A laboratory study of the minimum wind speed for wind wave generation, *J. Fluid Mech.*, *192*, 339–364, 1987.

Kitaigorodski, S., and M. Donelan, Wind-wave effects on gas transfer,

in *Gas Transfer at Water Surfaces*, edited by W. H. Brutsaert and J. Jirka, pp. 147–170, D. Reidel, Norwell, Mass., 1984.

Maat, N., C. Kraan, and W. A. Oost, The roughness of wind waves, *Boundary Layer Meteorol., 54*, 89–103, 1991.

Mahrt, L., D. Vickers, J. Howell, J. Edson, J. Hare, J. Højstrup, and J. Wilczak, Sea surface drag coefficients in RASEX, *J. Geophys. Res., 101*, 14,327–14,335, 1996.

Mahrt, L., D. Vickers, J. Edson, J. Wilczak, J. Hare, and J. Højstrup, Boundary-layer transitions in offshore flow, *Boundary Layer Meteorol., 100*, 3–46, 2001.

Moller, D., P. Mourad, and S. Frasier, Field observations of radar backscatter from the ocean surface under low wind speed conditions, *J. Geophys. Res., 105*, 24,059–24,069, 2000.

Nordeng, T. E., On the wave age dependent drag coefficient and roughness length at sea, *J. Geophys. Res., 96*, 7167–7174, 1991.

Paulson, C. A., The mathematical representation of wind speed and temperature profiles in the unstable atmospheric surface layer, *J. Appl. Meteorol., 9*, 857–861, 1970.

Perrie, W., and B. Toulany, Fetch relations for wind-generated waves as a function of wind-stress scaling, *J. Phys. Oceanogr., 20*, 1666–1681, 1990.

Piccirillo, P., and C. Van Atta, The evolution of a uniformly sheared thermally stratified turbulent flow, *J. Fluid Mech., 314*, 61–86, 1997.

Plant, W., W. Keller, V. Hesany, K. Hayes, K. Hoppel, and T. Blanc, Measurements of the marine boundary layer from an airship, *J. Atmos. Oceanic Technol., 15*, 1433–1458, 1998.

Plant, W., D. Weissman, W. Keller, V. Hessany, K. Hayes, and K. Hoppel, Air/sea momentum transfer and the microwave cross section of the sea, *J. Geophys. Res., 104*, 11,173–11,191, 1999.

Rieder, K. F., and J. A. Smith, Removing wave effects from the wind stress vector, *J. Geophys. Res., 103*, 1363–1374, 1998.

Smedman, A.-S., H. Bergström, and B. Grisogano, Evolution of stable internal boundary layers over a cold sea, *J. Geophys. Res., 102*, 1091–1099, 1997a.

Smedman, A.-S., U. Hogström, and H. Bergstrom, The turbulence regime of a very stable marine airflow with quasi-frictional decoupling, *J. Geophys. Res., 102*, 21,049–21,059, 1997b.

Smedman, A., U. Hogstrom, and H. Bergstrom, The marine atmospheric boundary layer during swell, according to recent studies in the Baltic Sea, in *Air-Sea Exchange: Physics, Chemistry and Dynam-*

ics, edited by G. L. Geernaert, pp. 175–196, Kluwer Acad., Norwell, Mass., 1999.

Sun, J., D. Vandemark, L. Mahrt, D. Vickers, T. Crawford, and C. Vogel, Momentum transfer over the coastal zone, *J. Geophys. Res., 106*, 12,437–12,448, 2001.

Toba, Y., and M. Koga, A parameter describing overall conditions of wave breaking, white capping, sea-spray production and wind stress, in *Oceanic Whitecaps*, edited by E. C. Monahan and G. Mac Niocaill, pp. 37–47, D. Reidel, Norwell, Mass., 1986.

Vickers, D., and L. Mahrt, Fetch limited drag coefficients over shallow water, *Boundary Layer Meteorol., 89*, 53–79, 1997a.

Vickers, D., and L. Mahrt, Quality control and flux sampling problems for tower and aircraft data, *J. Atmos. Oceanic Technol., 14*, 512–526, 1997b.

Vickers, D., and L. Mahrt, Observations of nondimensional shear in the coastal zone, *Q. J. R. Meteorol. Soc., 125*, 2685–2702, 1999.

Vickers, D., L. Mahrt, J. Sun, and T. Crawford, Structure of off-shore flow, *Mon. Weather Rev., 129*, 1251–1258, 2001.

Weissman, D., and H. Graber, Satellite scatterometer studies of ocean surface stress and drag coefficients using a direct model, *J. Geophys. Res., 104*, 11,329–11,335, 1999.

Wilczak, J. M., J. Edson, J. Højstrup, and T. Hara, The budget of turbulence kinetic energy in the marine atmosphere, in *Air-Sea Exchange: Physics, Chemistry and Dynamics*, edited by G. Geernaert, pp. 153–174, Kluwer Acad., Norwell, Mass., 1999.

Winstead, N., and G. Young, An analysis of exit flow drainage jets over the Chesapeake Bay, *J. Appl. Meteorol., 39*, 1269–1281, 2000.

T. L. Crawford and G. Crescenti, NOAA Air Resources Laboratory, Idaho Falls, ID 83402, USA.

P. Frederickson, Naval Postgraduate School, Monterey, CA 93943, USA.

L. Mahrt and D. Vickers, College of Oceanic and Atmospheric Sciences, Oregon State University, Corvallis, OR 97331, USA. (mahrt@oce.orst.edu)

J. Sun, National Center for Atmospheric Research, Boulder, CO 97331, USA.

Fluxes measured from moving platforms

L. Mahrt and Dean Vickers

COAS
Oregon State University
Corvallis, OR 97331 USA
mahrt@coas.oregonstate.edu

William Drennan and Hans Graber

Rosenstiel School of Marine and Atmospheric Science
University of Miami
Miami, FL, 33149, U.S.A.

Timothy L. Crawford
Air Resources Laboratory
NOAA
Idaho Falls, ID, 83402, USA

22 July 2002   .

Abstract

Errors in eddy correlation measurements from moving platforms (aircraft, ships, buoys, blimps, tethered balloons and kites) include contamination of the measured fluctuations by superficial fluctuations associated with vertical movement of the platform in the presence of mean vertical gradients. Such errors occur even with perfect removal of the motion of the platform. These errors are investigated here from eddy correlation data collected from the LongEZ research aircraft and ASIS buoy during the SHoaling Waves EXperiment.

1 Introduction

Except for towers, eddy correlation measurements of turbulent fluxes are generally made from moving platforms such as aircraft, buoys, ships and suspended platforms from tethered balloons, blimps, kites and aircraft. Errors in the measured velocity fluctuations occur due to incomplete removal of the platform motion, normally recorded with accelerometers, gyroscopes and differential GPS (Lenschow, 1986; Edson et al., 1998). Improvements in such systems are constantly reducing the errors associated with platform motion. Even with complete removal of platform motion, eddy correlation errors still occur due to the fact that the time series is not collected at a constant height above the mean surface and mean vertical gradients are normally not zero, particularly near the surface (Figure 1). Examples of vertical displacement are shown for the aircraft and buoy in Figure 2. As a result of the platform vertical displacements, superficial fluctuations may be generated by

2

the variation of the height of the measurement platform due to the vertical mean gradients. These errors were briefly examined in Lenschow (1973) and Vickers and Mahrt (1997), but otherwise are generally not considered in the literature. This study examines such errors in more detail. The errors due to platform vertical displacement are just one of a number of instrumental and sampling errors contaminating eddy correlation measurements from fixed or moving platforms (Moore, 1986; Mann and Lenschow, 1994; Mahrt, 1998 and Massman, 2000).

2   The data

For aircraft data, the errors due to vertical platform displacement are most easily examined over water where variations of surface elevation do not complicate the definition of height above ground. This study analyzes eddy correlation data collected from the LongEZ research aircraft over Atlantic coastal water off the Outer Banks near Duck, North Carolina during the SHOaling Waves EXperiment (SHOWEX) in March 1999 and November-December 1999 (Crescenti et al., 1999; French et al., 2000; Sun et al., 2001; Mahrt et al., 2001) using low-level aircraft data from 37 flights on 35 days at an average height of 15 m above the sea surface. The LongEZ is able to fly at this very low level for several hours at a time.

Fluxes are computed for 2 km segments of the aircraft legs using un-weighted averaging. For a wind of $5ms^{-1}$, this volume of air would pass a stationary platform in about 7 min. Records with negative moisture flux, upward momentum flux (presumably driven by swell), and flight levels above 25 m are excluded since some of the calculations will employ surface-layer similarity theory. Records are excluded where the absolute value of z/L ex-
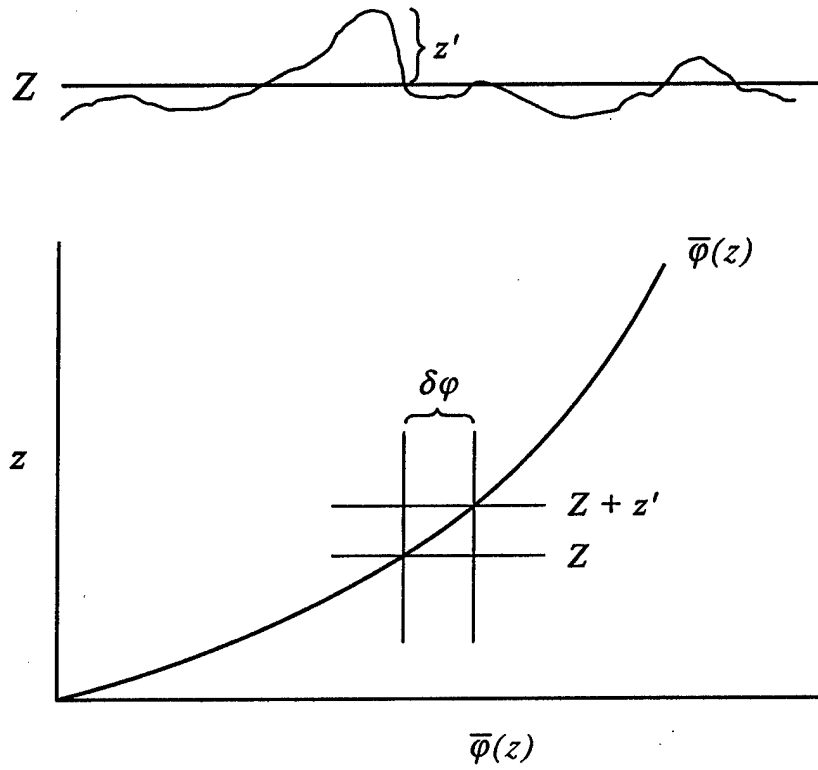
Figure 1: Geometry of superficial fluctuations due to vertical platform displacement in the presence of mean vertical gradients. The upper panel defines z' and Z for a hypothetical times series of platform height. The lower panel illustrates artificial fluctuations generated by vertical platform displacement in the presence of mean vertical gradients.
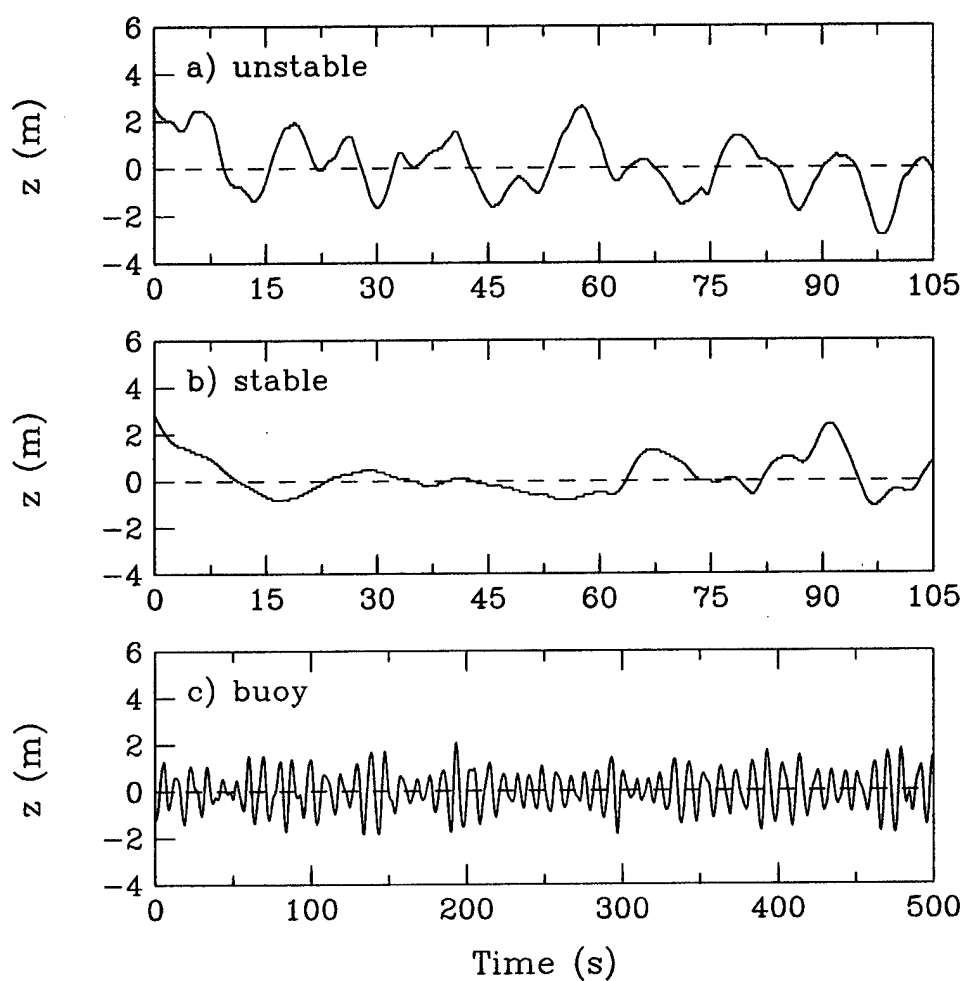
Figure 2: Examples of vertical displacement of the LongEZ for unstable conditions (a), stable conditions (b) and for the ASIS buoy for slightly stable conditions with 13 ms^{-1} mean wind and a large significant wave height of 4 metres (c).

ceeds five where fluxes may be strongly contaminated by flux sampling errors and where similarity theory is suspect. When computing bin-averaged values of ratios, such as the relative flux error (Section 5), for different intervals of stability, z/L, the values of the numerator and denominator are averaged first and then the ratio is computed. This procedure avoids ratio averaging problems where a few very large values of the ratio, due to small denominators, can dominate the average of the ratio. For some calculations, the data will be divided into stable and unstable classes. Here we exclude near neutral cases where the magnitude of z/L is less than 0.001.

The ASIS, or Air-Sea Interaction Spar buoy (Graber et al. 2000), is a partial surface follower, essentially following waves longer than 8 s. This latter property allows measurements within several metres of the interface in most conditions. The data used here are from the 'ROMEO' buoy during the SHOWEX experiment of autumn 1999. ROMEO is equipped with a 3-axis Gill R2A sonic anemometer, located on top of a mast at roughly 6m above mean sea level. The buoy is also equipped with a full motion package, allowing the measured wind velocities to be corrected for the motion of the platform. The instantaneous height of the anemometer above the surface is calculated from a capacitance wave staff positioned directly below the anemometer. For the calculations in this study, 30-minute records were selected every ten hours to provide a more manageable data set and to represent a cross-section of conditions during the 38 day deployment: $1 < U < 15ms^{-1}$ and $-2 < z/L < 1$. The fluxes are computed with unweighted averaging.

3 Platform displacement errors

Aircraft vertical displacement from a constant height above the surface is induced by turbulent updrafts and downdrafts and perhaps fluctuations of lift due to horizontal velocity fluctuations. Vertical displacement of buoys and ships is controlled by the surface wave field. The artificial fluctuations due to the height-variation of the observational platform for arbitrary variable ϕ (Figure 1) can be estimated as

$$\delta\phi(z') = z'(t)\frac{\partial\overline{\phi}}{\partial z} \tag{1}$$

where $\delta\phi(z')$ is the change of variable ϕ due to the vertical displacement of the platform from its mean elevation

$$z'(t) = z(t) - Z \tag{2}$$

where Z is the time-averaged height of the platform and $z(t)$ is the instantaneous height of the platform. Then any variable measured from the platform can be expressed as

$$\phi(z', t) = \phi(Z, t) + z'(t)\frac{\partial\overline{\phi}}{\partial z} \tag{3}$$

where $\phi(Z, t)$ is the desired instantaneous value measured at a fixed height. We will assume that the vertical mean gradient does not change significantly across the layer defined by $z'(t)$ and assume that the flow is stationary.

The vertical gradients may be large near the surface, resulting in significant artificial fluctuations, even if the change of platform vertical position is small. Are such artificial fluctuations sufficiently correlated with vertical velocity fluctuations to significantly alter the computed flux? To investigate

this issue, we expand the measured vertical flux as

$$\overline{w'(z,t)\phi'(z,t)} = \overline{w'(Z,t)\phi'(Z,t)} + \overline{w'(Z,t)\delta\phi(z')} + \overline{\delta w(z')\phi'(Z,t)} + \overline{\delta w(z')\delta\phi(z')}$$

$$(4)$$

where the overbar is a simple unweighted average in order to satisfy Reynolds averaging. The first term on the right hand side is the true vertical flux required for use in the basic conservation equation for $\overline{\phi}$. The remaining three terms on the right hand side are error terms. The last two error terms on the right hand side are related to heterogeneity of the mean flow through mass continuity in that artificial fluctuations of vertical velocity are proportional to $\partial\overline{w}/\partial\overline{z}$ (Eq. 1). These terms vanish for homogenous flow. Even if the platform was motionless with no vertical displacement, the estimate of the first term on the right hand side of Eq. 4 from finite records contains a random flux error due to variability of the turbulence.

4 Vertical velocity correlation term

The second term on the right hand side is due to the correlation between the vertical velocity fluctuations and the artificial fluctuations of ϕ. Estimating the $\delta\phi(z')$ from Eq. 1, this term becomes

$$\overline{w'(Z,t)\delta\phi(z')} = \overline{w'(Z,t)z'(t)}\frac{\partial\overline{\phi}}{\partial z}. \tag{5}$$

To numerically estimate this error term, $w'(Z,t)$ is approximated by $w'(z',t)$. Below, $\phi'(Z,t)$ will be approximated by $\phi'(z',t)$. Such approximations correspond to only higher order errors, which are small compared to $\overline{w'(Z,t)\delta\phi(z')}$ provided that z' is not too large.

8

The vertical gradient, $\partial \bar{\phi}/\partial z$, can be estimated in two ways. In the first approach, it is estimated by regressing $\phi'(z', t)$ on z. A potential difficulty of this "regression" approach is that the platform height might be correlated with the turbulence itself, in which case the estimated value of $\partial \bar{\phi}/\partial z$ is contaminated by turbulent fluctuations.

In the second approach, the vertical gradient $(\partial \bar{\phi}/\partial z)$ is estimated from similarity theory as

$$\frac{\partial \bar{\phi}}{\partial z} = \frac{\Phi_\phi(Z/L)\phi_*}{\kappa Z} \tag{6}$$

where L is the Obukhov length, κ is the von Karman "constant", $\Phi_\phi(Z/L)$ is the specified stability function for variable ϕ and

$$\phi_* \equiv -\frac{\overline{w'(Z,t)\phi'(Z,t)}}{u_*} \tag{7}$$

and u_* is the true surface friction velocity. Substituting Eqs. 6-7 into Eq. 5, we obtain

$$\overline{w'(Z,t)\delta\phi(z')} = \overline{w'(Z,t)z'(t)\frac{\Phi_\phi(z/L)\overline{w'(Z,t)\phi'(Z,t)}}{\kappa z u_*}}. \tag{8}$$

Dividing this relationship by the flux computed from a stationary platform, the relative error can be written as

$$\overline{w'(Z,t)z'(t)}\frac{\Phi_\phi(z/L)}{\kappa z u_*}. \tag{9}$$

In the surface layer, Φ_ϕ for heat, moisture and momentum decreases slowly with increasing instability and increases with stability. The principal uncertainty with this "similarity" estimate of the vertical gradient is errors in the similarity relationship with strong stability, advection, and nonstationarity and possible location of the platform within the wave boundary layer (roughness sublayer over land).

9

5 Displacement flux errors for the aircraft

The displacement flux error depends on record length, method of estimation of the vertical gradient and atmospheric stability. The estimate of the vertical gradient $\partial\overline{\phi}/\partial z$ based on regressing $\phi'(z', t)$ on z for the LongEZ data produces larger vertical gradients than the similarity prediction of the vertical gradient and therefore larger estimates of the displacement error. We will focus on estimates based on similarity theory because the error estimates are less variable. Furthermore, it is not possible to isolate the influence of correlation between turbulence quantities and z' that would contaminate the estimation of the vertical gradient based on the regression method.

5.1 Random and systematic contributions

The dependence of the displacement error on the record length is partly due to the fact that a substantial fraction of the displacement flux error is random. We can theoretically express the displacement error for a particular record as

$$DE = [SE] + RE \tag{10}$$

where $[SE]$ is the systematic part of the displacement error and RE is the random part of the displacement flux error. The total displacement error approaches the systematic error as the sample size becomes large, assuming that the sample is homogeneous. This random error is different from the random flux error associated with the estimate of the desired flux for a level platform (first term on the right hand side of Eq. 4). The latter is due to the random distribution of transporting eddies and is always present. We refer to this random error simply as the "random flux error" as opposed to the random part of the displacement error. It is traditionally estimated for

10

homogeneous records as the standard deviation of the 200-m flux, σ_F, divided by the square root of the number of 200 m subrecords, N

$$RFE = \frac{\sigma_F}{\sqrt{N}} \qquad (11)$$

Subrecords of 200 m omit some of the flux for unstable conditions but the intention here is to capture enough subrecords to estimate the standard deviation of the flux. For the present analysis of aircraft data, we evaluate the error term from 2 km records (Section 2), which is smaller than the usual aircraft record length of 10 km or longer. The random flux error and the random part of the flux displacement error both decrease with increasing record length, as will be verified below. In this sense, the following analysis for $2km$ records provides an upper bound for the two random errors.

5.2   Observed distribution

We now examine the behavior of the displacement error normalized by the flux for a stationary platform, as estimated from Eq. 9. The frequency distribution of this relative displacement error does indeed suggest that the random part of the displacement error is substantially larger than the systematic error (Figure 3). The frequency peak of the relative flux displacement error for both heat and momentum fluxes appears to be positive for stable conditions with a value of a few percent, within the uncertainty of the relatively crude resolution of the frequency distribution. The positive values of the relative displacement error correspond to artificial augmentation of the computed flux. Since the expected mean of the random part of the displacement error is zero, this suggests that the relative systematic error is positive with a magnitude of a few percent for stable conditions. Based on the frequency distribution, the relative systematic error for unstable conditions also

appears to be positive, but cannot be safely distinguished from zero (Figure 4).

As a quantitative estimate of the displacement error we average the relative displacement error (retaining the sign) for all of the 2 km segments (approximately 560 km of total data) within a stability class. The averaged value of the relative displacement error for stable conditions is +4% for heat and +2% for momentum. The corresponding values are only +0.5% for unstable conditions for both heat and momentum fluxes. For unstable conditions, the relative errors are much smaller, partly due to larger absolute values of the fluxes and partly because the vertical gradients at the aircraft level are generally smaller in the unstable case (thinner surface layer).

As the record length increases from 2 km to 20 km, the random part of the displacement error is expected to decrease by a factor of $1/\sqrt{10}$. For 20 km records (not shown), the magnitude of the relative displacement error is substantially smaller than that for 2 km and rarely exceeds 5%. The relative flux displacement error increases with increasing stability, although the scatter is too large to confidently formulate such a dependence. The relative errors are generally largest for very stable conditions, where the flux magnitudes are small.

5.3 Origin of displacement error

The positive average values of the relative displacement error for stable stratification result from a negative correlation between the atmospheric vertical velocity and the aircraft displacement. The covariance is also generally negative for unstable conditions where the averaged relative displacement error is very small. Theoretically, one might postulate that the covariance should be zero because the aircraft displacement, z' would reach its maximum positive
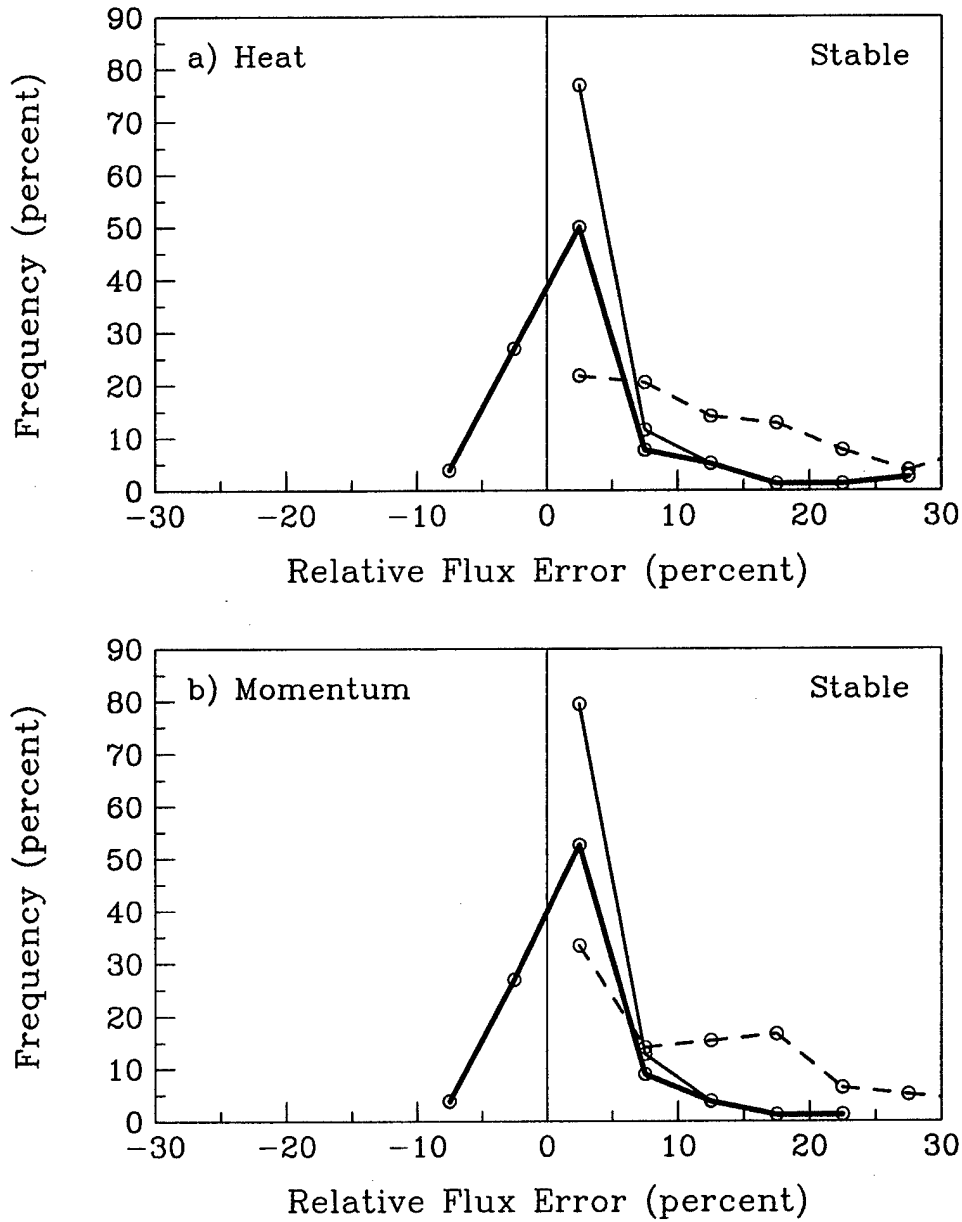
12

Figure 3: The frequency distribution of the relative displacement error (thick solid), the absolute value of the relative displacement error (thin solid) and the random flux error estimated from Eq. 11 (dashed) for the LongEZ aircraft data for stable conditions for heat fluxes (a) and momentum fluxes (b).
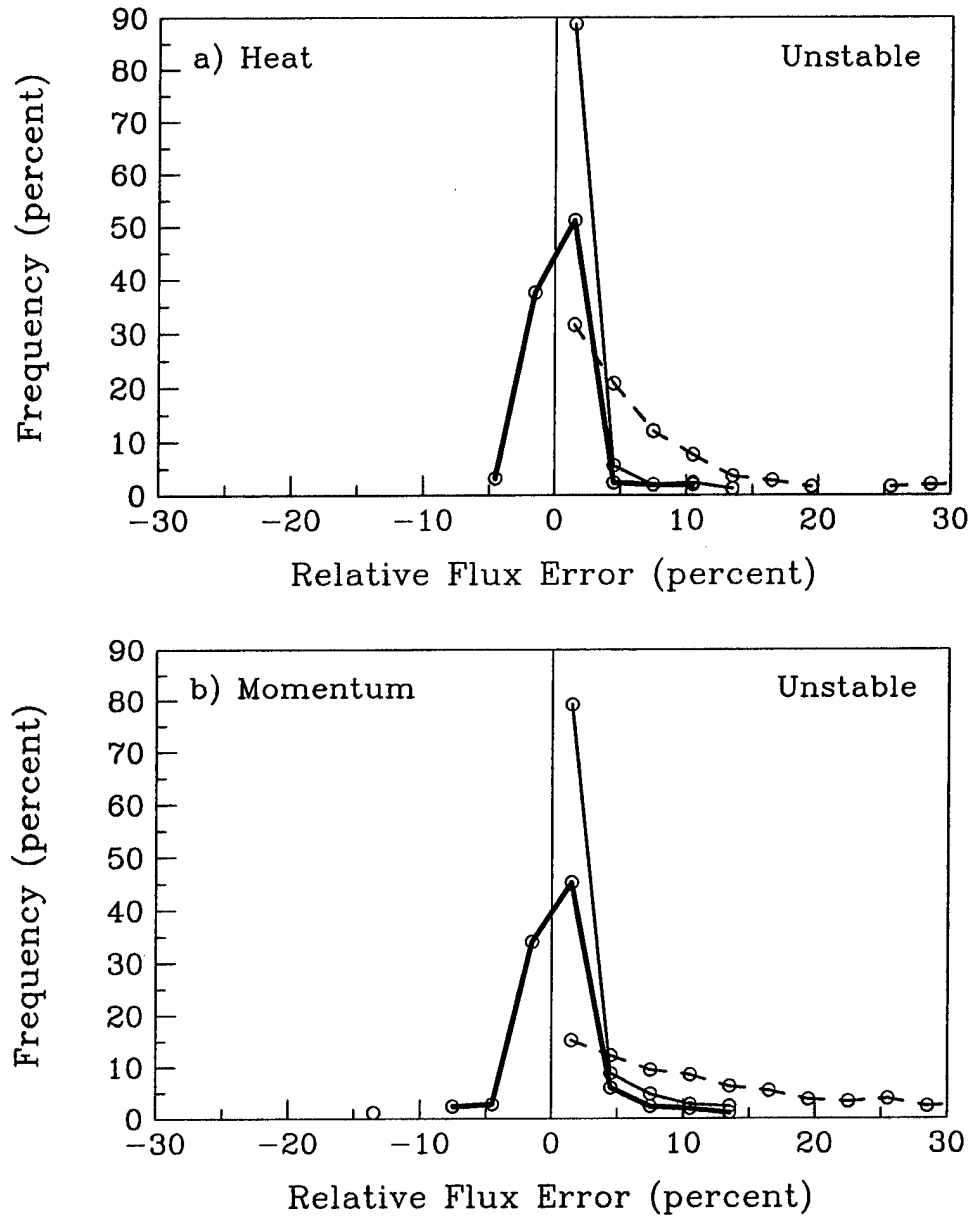
Figure 4: The frequency distribution of the relative displacement error (thick solid), the absolute value of the relative displacement error (thin solid) and the random flux error estimated from Eq. 11 (dashed) for the LongEZ aircraft data for unstable conditions for heat fluxes (a) and momentum fluxes (b)

value as the updraft to downdraft motion, and so forth. Indeed, the actual correlations between the vertical velocity and the displacement for individual records average only about -0.03, but the correlation is negative for most of the records. The correlation is very small but systematic. The negative correlation suggests an overall lag in the aircraft response to updrafts and downdrafts, which might be influenced by the skewness of the vertical velocity fluctuations, pilot response characteristics and aircraft aerodynamics. We conclude that the flux displacement error for short aircraft records is strongly influenced by the random part of the displacement error but is smaller than the usual random flux error and therefore of limited significance. For longer records, the systematic part of the displacement error is dominant, but is only a few percent of the total flux depending on stability and the transported quantity.

5.4   Random flux error

The random flux error is by definition positive but can be compared to the frequency distribution of the absolute value of the displacement error (Figures 3 and 4, thin solid lines). As an example, the probability of significant relative displacement error greater than 10% is much less than that for the random flux error. The averaged random flux error is about three times greater than the absolute value of the displacement error for both heat and momentum fluxes for stable conditions and an order of magnitude greater than the absolute value of the displacement error for unstable conditions. For individual 2-km records, the random flux error is greater than the total displacement error for 90% of the records for both heat and momentum for the stable case while the random flux error is greater than the total displacement error for all of the records for the unstable case.

6 Buoy displacement flux errors

For ships and buoys, the height of the platform, $z(t)$, of the platform may also correlate with $w'(z, t)$ since eddies in the wave boundary layer exhibit phase relationships with the surface waves (e.g. Hare et al., 1997). Eddy correlation measurements are best taken above the wave boundary layer, in the surface layer, where Monin-Obukhov similarity theory potentially applies and such platform-induced errors should be smaller since the vertical displacement of the buoy and the atmospheric vertical velocity should become less correlated.

For a given value of the Obukhov length, the vertical gradients should be larger for the buoy since the buoy measurement level is closer to the surface (6 m compared to about 15 m for the aircraft). However, the relative displacement flux errors are not generally larger for the buoy, partly because both the atmospheric vertical velocities at the buoy observational level and the platform displacements are both generally smaller for the buoy compared to those for the aircraft.

The details of the above results are influenced by the definition of the zero reference height for the buoy. The platform height is separately computed with respect to the distance of the instrument from the mean water height and with respect to the distance from the instantaneous wave field. The latter is affected mainly by short waves since the buoy rides the long waves; that is, z becomes defined as the height above the long waves (swell). The influence of buoy tilt on the distance between the sensor height and wave surface is small. The eddies in the surface layer integrate out the influence of the shorter waves (by definition of the surface layer) so that the correlation between the turbulent vertical fluctuations and the short waves should be zero. The displacement flux errors for heat are approximately the same in

both coordinate systems but the momentum displacement error averages an order of magnitude smaller using the instantaneous height. In the following, we employ height above mean sea level because it is a little easier to interpret, does not depend on the wave riding ability of the buoy and serves as a maximum error estimate.

The correlation between the buoy displacement height and $w'(z', t)$ is larger than that for the aircraft, but still averaging only -0.15. This correlation may be due to the atmospheric streamlines following the long waves. This possibility corresponds to location of the buoy within the wave boundary layer for the long waves. The displacement flux errors for the buoy depend on wave height through the influence on z' and depend on atmospheric stability through the influence on the vertical gradients. The data was partitioned into intervals of small and large significant wave height (rms of wave height greater than or less than 1.5 m) and further subdivided into stable and unstable classes. Sufficient data was available only for the unstable class. The relative errors for the momentum flux (Figure 5) are shifted towards larger values for the class of large significant wave height. The random part of the error, as indicated by the spread, is less than that for the aircraft (Figures 3-4) because the buoy records are relatively longer (Section 2). The relative displacement error for the heat flux does not show the same sensitivity to the wave height as that for momentum (Figure 5), perhaps because scalar fields due not directly respond to pressure fluctuations induced by the large errors. Even for large waves, the relative displacement error for both fluxes are relatively unimportant. The displacement error artificially increases the heat flux and decreases the momentum flux and, therefore, artificially increases $-z/L$.
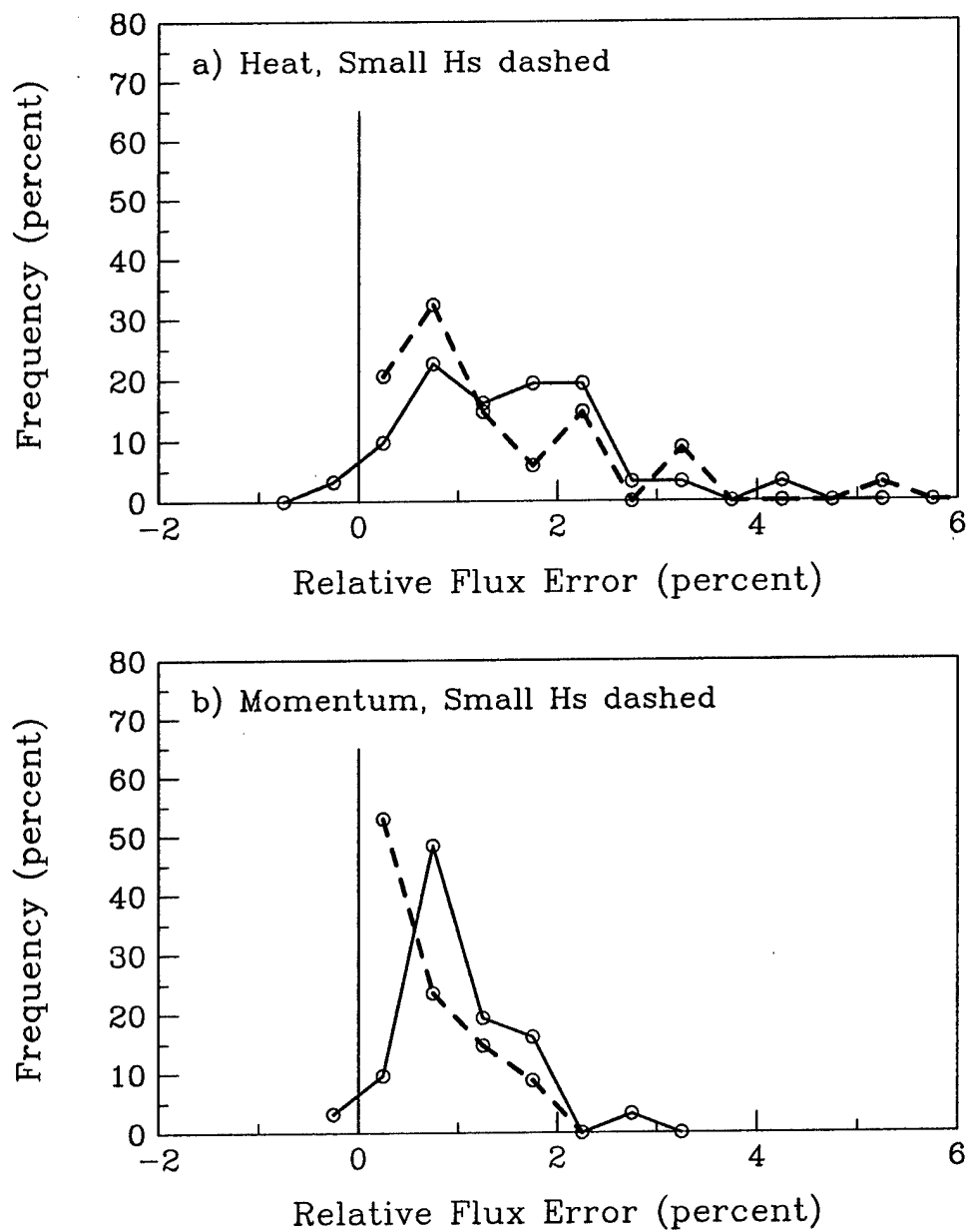
17

Figure 5: The frequency distribution for the relative displacement flux error for the ASIS buoy for unstable conditions for heat (upper panel) and momentum (lower panel) where the solid line represents the class of large significant wave height and the dashed line represents the class of small significant wave height.

18

7 Heterogeneity terms

The third term on the right hand side of Eq. 4 can be expressed as

$$\frac{\partial \overline{w}}{\partial z} \, \overline{z'(t)\phi'(Z,t)} \tag{12}$$

where we have estimated $\delta w(z')$ from Eq. 1 in terms of the mean vertical gradient and platform displacement z'. For some applications, the horizontal divergence of the wind field might be more easily estimated than the vertical divergence of the vertical velocity. Using incompressible mass continuity, Eq. 12 becomes

$$-\frac{\partial \overline{u}}{\partial x} \, \overline{z'(t)\phi'(Z,t)} \tag{13}$$

Here, x is assumed to be the primary direction of horizontal divergence $\partial \overline{v}/\partial y \approx 0$.

As an example, consider the case where the platform is a light aircraft and ϕ is the horizontal wind component for offshore accelerating flow, corresponding to horizontal divergence. With a head wind (tail wind), horizontal wind gusts increase (decrease) the lift and z', in which case the correlation is positive (negative) and the flux correction term for momentum is negative (positive). That is, the computed downward momentum flux is artificially enhanced with a headwind and reduced with a tailwind. This term was evaluated from flights perpendicular to the coast by estimating the horizontal gradient of the wind in terms of linear regression over 2 km segments. The term was small for both heat and momentum, generally less than 2% of the total flux. This term could be potentially important near surface discontinuities, such as flow immediately downstream from the coastline or over heterogeneous land surfaces. However, the flux calculation based on aircraft

19

measurements becomes ambiguous over strong surface heterogeneity in that horizontal variations of the mean flow contaminates the computed turbulent fluctuations. This heterogeneity term could also be large with transient disturbances but significant influences are probably limited to fronts and convective cloud systems. We conclude that for the present data, this heterogeneity term is small for the heterogeneity encountered in SHOWEX.

Applying Eq. 1 to the fourth term on the right hand side of Eq.4, we obtain the scaling estimate

$$\overline{\delta w(z')\delta\phi(z')} = \frac{\partial \overline{w}}{\partial z}\frac{\partial \overline{\phi}}{\partial z}\overline{z'^2} \tag{14}$$

Again using incompressible mass continuity

$$\overline{\delta w(z')\delta\phi(z')} = -\frac{\partial \overline{u}}{\partial x}\frac{\partial \overline{\phi}}{\partial z}\overline{z'^2} \tag{15}$$

This term can be of either sign depending on whether the flow is accelerating or decelerating. This term is also found to be quite small.

8 Error in mean values

An error in the mean profiles due to platform displacements occurs when the mean gradients are not constant with height. The mean flow measured on a moving platform can be expressed as

$$\overline{\phi(Z + z',t)} = \int_0^\infty \overline{\phi}(Z + z')f(Z + z')d(Z + z') \tag{16}$$

where Z is again the averaged height of the platform and z' is the deviation of the platform height from Z and $f(Z + z')$ is the frequency distribution of the height of the platform. Even if $f(Z + z')$ is a symmetric function of z', the time-average value of $\overline{\phi(Z + z',t)}$ will normally differ from the

20

average at a fixed height, Z, because the time-averaged value of $\overline{\phi}$ is usually a nonlinear function of height. Since the mean shear decreases with height, the mean wind speed on a moving platform will be underestimated. That is, negative $z'(t)$ induces larger artificial fluctuations than positive $z'(t)$. The net effect of this error causes underestimation of the mean wind speed, which in turn cause overestimation of the drag coefficient and roughness length.

An order of magnitude estimate of potential errors due to platform displacement can most easily be constructed for the case of neutral stability with a logarithmic wind profile

$$\overline{u(z,t)} = \frac{u_*}{\kappa} ln\frac{z}{z_o} \tag{17}$$

where z retains traditional meaning and z_o is the aerodynamic roughness length, assumed to be small compared to the observational height. As the simplest possible estimate, assume the aircraft flies 50% of the time at level z_1 and 50% of the time at level z_2, so that the measured average wind speed for sufficiently long record length is

$$\overline{u(Z + z',t)} = \frac{u_*}{2\kappa}(ln\frac{z_1}{z_o} + ln\frac{z_2}{z_o}). \tag{18}$$

Noting that the true averaged wind speed for the average flight level can be expressed as

$$\overline{u(z,t)} = \frac{u_*}{\kappa} ln\frac{(1/2)(z_1 + z_2)}{z_o}, \tag{19}$$

the ratio of the measured wind speed to the true wind speed is

$$\frac{(1/2)(lnz_1 + lnz_2) - lnz_o}{ln(z_1 + z_2) - ln(2z_o)} \tag{20}$$

Incrementally varying z_1 and z_2, corresponding to mean height variations between 4 and 20 m and height differences between 0 and 5 m, the relative

21

platform error is found to be substantially less than 1%. This result was supported by numerically integrating Eq. 16 for the case of a Gaussian distribution of platform errors. Even for a mean observational height of 2 m and displacements of 1m about the mean (corresponding to a 2 m wave height for waves greater than 8 s), the mean wind is underestimated by only 1%.

Defining the error in wind speed as

$$\epsilon \equiv \overline{u(Z + z', t)} - \overline{u(Z)} \qquad (21)$$

the drag coefficient estimated from a moving platform is

$$\frac{\overline{w'u'}}{\overline{u(Z, t)}^2 + 2\epsilon\overline{u(Z, t)} + \epsilon^2}. \qquad (22)$$

Expanding the denominator in terms of a Taylors expansion, the percentage error in the drag coefficient due to errors in the mean wind is 2ϵ to lowest order. For example, a 1% underestimation of the mean wind leads to a 2% overestimation of the drag coefficient. We conclude that the effect of platform displacement on the mean wind and drag coefficient is not important.

9   Conclusions

We have studied the impact of errors due to vertical displacement of platforms resulting from contamination of the computed turbulent fluctuations by mean vertical gradients. Aircraft platform fluctuations for the present data lead to small overestimation of the heat and momentum fluxes for stable conditions and unimportant errors for unstable conditions. For typical record lengths, the magnitude of the displacement flux error is generally smaller than the usual random flux error, where the latter remains nonzero even for stationary platforms. Both random errors are reduced by increasing record length.

The displacement flux error can be theoretically partitioned into a random part (not to be confused with the usual random flux error) and a systematic part. The flux displacement error for short aircraft records is strongly influenced by the random part of the displacement flux error, which is smaller than the usual random flux error. For longer aircraft records, the random part of the displacement flux error decreases and the displacement flux error approaches the small systematic part of the error, typically a few percent of the total flux for stable conditions and less than one percent for unstable conditions. The systematic error tends to increase with stability. The general unimportance of the displacement error for the LongEZ is encouraging since this small aircraft is displaced more by atmospheric vertical velocity fluctuations compared to larger aircraft. Larger aircraft are unable to fly as close to the sea surface and are therefore less suitable for estimating surface fluxes in thin stable boundary layers over the sea. For flight levels closer to sea surface, the flux displacement error is expected to be larger because of larger vertical gradients. Unmanned aircraft may suffer larger platform displacement errors because of larger vertical displacements.

Compared to the aircraft, the buoy errors would be enhanced by stronger gradients at the lower observational levels of the buoy, but are reduced by small magnitudes of the buoy displacement and the small vertical velocities close to the surface. The displacement flux error for the buoy becomes marginally significant only for large wave heights where it averages a few percent.

Acknowledgments

References

Crescenti, G.H., T.L. Crawford, and E.J. Dumes, Data Report: Long EZ(N3R) participation in the 1999 shoaling waves experiment(SHOWEX) pilot study. NOAA Technical Memorandum ERL ARL- 232, Silver Spring, MD, 86, 1999.

Edson, J., A. Hinton, K. Prada, J. Hare, and C. Fairall, 1998: Direct covariance flux estimates from mobile platforms at sea. *J. Atmos. Oceanic Tech.* , **15**, 547-562.

French J.R., G.H. Crescenti, T.L. Crawford and E.J. Dumas, Long EZ participation in the 1999 shoaling waves experiment (SHOWEX), NOAA Data Report OAR ARL-20, Silver Spring, MD, 51, 2000.

Graber, H.C., E.A. Terray, M.A. Donelan, W.M. Drennan, J. Van Leer and D.B. Peters, 2000: ASIS – A new air-sea interaction spar buoy: design and performance at sea. *J. Atmos. Oceanic Tech.* , **17**, 708-720.

Hare, J. E., T. Hara, J. B. Edson, and J. M . Wilczak, 1997: A similarity analysis of the structure of airflow over surface waves. *J. Phy. Oc.*, **27**, 1018-1037.

Lenschow, D. H., 1973: Two examples of planetary boundary layer modification over the Great Lakes. *J. Atmos. Sci.*, **30**, 568-581.

Lenschow, D. H., 1986: Aircraft Measurements in the Boundary Layer. A chapter in *Probing the Atmospheric Boundary Layer*, edited by D. H. Lenschow, American Meteorological Society, Boston, MA, 39–55.

Mahrt, L., 1998: Flux sampling strategy for aircraft and tower observations. *J. Atmos. Oceanic Tech.* , **15**, 416-429.

Mahrt, L., D. Vickers, J. Sun, T. Crawford, G. Crescenti, and P. Frederickson, 2001: Surface stress in offshore flow and quasi-frictional decoupling. *J. Geophys. Res.*, **106**, 20,629-20,639.

Mann, J. and D. H. Lenschow, 1994: Errors in airborne flux measurements. *J. Geophys. Res.*, **99**, 14,519-14,526.

Massman, W. J., 2000: A simple method for estimating frequency response corrections for eddy covariance systems. *Agric. For. Meteorol.* , **104**, 185-198.

Moore, C. J., 1986: Frequency Response Corrections for Eddy Correlation Systems, *Boundary-Layer Meteorol.*, **37**, 17-35.

Vickers, D. and Mahrt, L., 1997: Quality control and flux sampling problems for tower and aircraft data, *J. Atm. and Oc. Tech.*, 14, 512-526.

Sea-surface aerodynamic roughness

L. Mahrt and Dean Vickers
COAS
Oregon State University
Corvallis, OR 97331 USA
mahrt@coas.oregonstate.edu

Paul Frederickson and Ken Davidson
Naval Postgraduate School
Monterey, CA, 93943 USA

Ann-Sofi Smedman
Dept. of Meteorology
U. of Uppsala
S-752 36 Uppsala, Sweden

7 Feb 2003

Abstract

This study surveys and evaluates similarity theory for estimating the sea-surface drag coefficient with the bulk aerodynamic method. The most commonly used formulations of the aerodynamic roughness length, required by similarity theory, are examined using data sets from four different field programs. These relationships include the Charnock formulation and the wave age modified Charnock relationship. The goal is to assess the overall performance of simple formulations of the roughness length including cases where the Charnock formulation is not expected to apply. The goal is to assess the errors resulting from application of the Charnock formulation to all conditions, as is done in many numerical models where an explicit wave model cannot be accommodated.

This examination indicates that spurious self-correlation explains more variance than actual physical relationships, even after eliminating weak wind cases. Frequent cases of anomalously low stress and very small values of the Charnock coefficient further reduce the usefulness of this formulation for the present data sets. Causes of the frequent very small values of the Charnock coefficient are briefly investigated.

1   Introduction

The surface stress over the sea is normally formulated in terms of a drag coefficient based on the aerodynamic roughness length for momentum for the sea surface (hereafter referred to as the roughness length) and the stability functions for Monin-Obukhov similarity theory (e.g., Donelan, 1990). While there are common conditions where Monin-Obukhov similarity theory does not apply, the fact that the sea surface is a moving surface, by itself, does not preclude application of Monin-Obukhov similarity theory in the surface layer. Monin-Obukhov similarity theory often approximates the behavior of the turbulence energy budget (Edson and Fairall, 1998; Wilczak et al., 1999) and flux-gradient relationship (Vickers and Mahrt, 1999) as long as the observations are in the surface layer, above the wave boundary layer (e.g. Hare et al., 1997). With weak winds and swell, a surface layer where Monin-Obukhov similarity theory is valid cannot be identified (Smedman et al., 1999; Grachev and Fairall, 2001).

After reviewing a generalized similarity theory applied to the sea surface (Section 2), Section 3 discusses different formulations of the roughness length. Data sets for evaluation of parameterization of the roughness length are described in Section 4. The strong role of self-correlation in the parameterization schemes is studied in Section 5. The large variability of the Charnock coefficient between data sets and wind speed and wave age regimes is studied in Section 6. Our goal is to assess the errors resulting from application of the Charnock relationship to a wide variety of conditions, as is done in most regional and large-scale models, cannot accommodate the complexity and computer time required for a wave model. To construct such an assessment, we will not removed common cases of swell or other conditions where the Charnock relationship is not expected to apply.

2 General similarity theory

Formulation of momentum transfer in the atmosphere adjacent to the surface is often expressed in terms of an inverse flux-gradient relationship, referred to as the nondimensional shear

$$\phi_m \equiv \frac{\kappa z}{u_*} \frac{\partial u}{\partial z} = f(z/L, Re_*, z/\lambda, z/h, G) \tag{1}$$

where the far right hand side includes suspected possible influences on the flux-gradient relationship for stationary homogeneous flow. Here, Re_* is the roughness Reynolds number, λ is a length scale for the waves, h is the boundary-layer depth and G is a functional dependence on additional influences, all discussed in this section. L is the Obukhov length, which represents the influence of atmospheric stability on generation or inhibition of turbulence near the surface. If only the first argument on the right hand side is retained, Eq. 1 reduces to Monin-Obukhov similarity theory.

A more practical formulation for the surface stress is traditionally constructed by solving for the surface friction velocity and vertical integrating the nondimensional gradient from the observation level to near the surface, in which case the drag coefficient is formulated as

$$C_d \equiv \frac{u_*^2}{U^2} = F(\ln \frac{z}{z_o}, z/L, Re_*, z/h, z/\lambda, G) \tag{2}$$

where U is the wind speed computed from the time-averaged wind components at the observational level.

3

The lower limit of integration is z_o, the aerodynamic surface roughness length. This is the level at which the wind predicted by Eq. 2 with only z/L and $ln(z/z_o)$ as arguments, vanishes when extrapolating toward the surface. The roughness length has not been rigorously formulated for cases where other arguments ($Re_*, z/h, z/\lambda, G$) become important, although additional influences are sometimes "added" to traditional formulations, discussed below.

The near-surface flow can be divided into the wave boundary layer adjacent to the surface and the overlying surface layer. In the wave boundary layer (e.g., Hare et al., 1997), the flux-gradient relationship depends on length scales associated with the geometry of the surface. The influence of the wave length scales become unimportant in overlying surface layer where Monin-Obukhov similarity theory may be valid. The wave length scale, represented by λ in Eq. 1, is sometimes chosen as the wavelength or wave height of the dominant waves or some scale derived from the wave spectra. With concurrent wind-driven waves and swell, the statistical analysis of Rieder and Smith (1998) suggests that the stress vector is rotated from the wind vector by any swell that propagates in a direction significantly different from the wind direction, invalidating Monin-Obukhov similarity theory. Grachev and Fairall (2001) found that the influence of swell on the surface stress was particularly large for weak wind conditions, causing the wind and stress directions to be different.

The roughness Reynolds number, Re_*, represents the influence of smooth flow viscous effects (e.g. Brutsaert, 1982), which may become important in weak wind cases. Related influences include surface tension and surfactants, which are most likely to be important in weak wind conditions. As a result of the multitude of complications for weak wind conditions, the data analysis in Section 5 will first be conducted without weak wind conditions.

With thin atmospheric boundary layers, the influence of the boundary-layer depth, h, on the flux-gradient relationship may extend downward to the surface. For example, Mahrt et al. (1998) found that the shallow depth of the internal boundary layer in offshore flow over warm water restricted the development of large convective eddies, causing the transfer coefficient to be smaller than that predicted by Monin-Obukhov similarity theory. This argument was extended to the nondimensional shear in Vickers and Mahrt (1999).

The effect of the stability is particularly strong in near-collapse of the turbulence in warm air advection over cooler water (Smedman, 1997a,b; Mahrt

et al., 2001a,b) where Monin-Obukhov theory may not be applicable, or applicable only in a thin surface layer below traditional observational levels. If the influence of the boundary-layer depth extends down to the wave boundary layer, then a surface layer where Monin-Obukhov theory applies, does not exist.

Other influences, not explicitly represented above, may become important in special situations and are collectively included in the argument G. Such influences include nonstationarity and baroclinity (thermal wind) (Geerneart, 1996). Advection of stronger turbulence from land can also alter the flux-gradient relationship immediately downstream from the coast (Vickers et al., 2001). With shear instability above thin stable boundary layers, turbulence energy may be transported downward toward the surface and alter the flux-gradient relationship near the surface (Mahrt et al., 2001a,b).

Sorting out the various influences on the flux-gradient relationship is not normally possible with existing data and progress has been made only when several of the above influences can be neglected. The most notable case is Monin-Obukhov similarity theory where all of the above arguments on the right hand side of Eq. 2 can be neglected except z/L and lnz/z_o. Then the drag coefficient can be formulated with Monin-Obukhov similarity theory as

$$C_d = \frac{u_*^2}{U^2} = [\frac{\kappa}{ln(z/z_o) - \psi_m}]^2. \tag{3}$$

The stability function, ψ_m, must be specified as a function of z/L. We choose the formulations from Paulson (1970) for the unstable case and Dyer (1974) for the stable case. Given observed fluxes and mean wind, the roughness length can be computed from Eq. 3. The roughness length computed from observations can be contaminated by either failure of Monin-Obukhov similarity theory due to influences discussed above or inaccurate specification of ψ_m, as might be expected in very stable conditions. In these cases, the relationship between the estimated roughness length and actual roughness of the waves becomes obscure (Sun et al., 2001). Numerical models are required to apply Monin-Obukhov similarity to all situations because suitable alternatives do not exist.

In cases where no information is available on wave state, the roughness length is often formulated in terms of the Charnock formulation (Charnock, 1955) with constant coefficient, as is applied in the commonly used TOGA COARE algorithm (Fairall et al., 1996) as well as numerous other models.

5

Is it possible to improve upon this scheme without any information on wave state?

3 Formulation of the aerodynamic roughness length

The roughness length is computed from Eq. 3 using the observed fluxes and wind speed and stability functions. The computed roughness length assumes that the stability functions are correct, the measured quantities are correct and that they are measured in the surface layer, above the wave boundary layer. Otherwise, the physical interpretation of the roughness length becomes vague since it must compensate for inadequacies in the data or for all of the influences not included in Monin-Obukhov similarity theory; that is, the last four arguments on the right hand side of Eq. 2.

A goal of this study is to evaluate the applicability of the Charnock relationship. The Charnock formulation is a common parameterization of the aerodynamic roughness length over the water, which does not explicitly incorporate information on wave state. This relationship has been applied to snow and ice surfaces as well (Andreas and Claffey, 1995). It is written as

$$z_o = \alpha \frac{u_*^2}{g} \qquad (4)$$

where α is the Charnock coefficient, often referred to as a nondimensional roughness length. This formulation assumes that the influence of wave state on the roughness length is represented by the surface stress.

For neutral conditions (no buoyancy flux), one can combine Eq. 3 with the Charnock parameterization to obtain

$$z_o ln(\frac{z}{z_o})^2 = \frac{\alpha \kappa^2}{g} U^2 \qquad (5)$$

Since the left hand side of Eq. 5 is an increasing function of the roughness length, this relationship predicts that the roughness length increases with wind speed. Since this increase is counter to observational tendencies for weak wind conditions, the Charnock relationship with constant coefficient cannot be used for weak wind conditions, even as a first approximation (Section 6).

6

Sometimes the roughness length is defined in terms of the Charnock term (Eq. 4) and a smooth flow term in which case the Charnock coefficient is computed as (e.g., Fairall et al., 1996)

$$\alpha_s = (z_o - 0.11\frac{\nu}{u_*})\frac{g}{u_*^2} \tag{6}$$

For weak wind speeds or small roughness Reynolds number, this value of the Charnock coefficient can be substantially less than the traditional value (Eq. 3). Except when specified otherwise, we will use the original definition of the Charnock coefficient (Eq. 4).

The Charnock relationship is often generalized by introducing a dependence on wave age as in Toba and Koga (1986), Maat et al. (1991), Donelan (1990) and Smith et al. (1992). This dependence can be expressed as

$$\alpha = K(\frac{u_*}{C_p})^p \tag{7}$$

where K and p are empirical parameters and C_p is the phase speed of the dominant waves. Recall that dependence of the roughness length on wave state is compatible with Monin-Obukhov similarity theory while direct dependence of the flux-gradient relationship on wave scales (such as λ) is not compatible. Recently, Drennan et al. (2002) analyzed data from five field programs and found overall values of $K = 1.59$ and $p = 1.67$. Incorporating this expression for the Charnock coefficient into Eq. 4

$$z_o = K(\frac{u_*^2}{g})(\frac{u_*}{C_p})^p. \tag{8}$$

where $p = 1$.

Donelan (1990) scaled the roughness length with the rms wave height and related it to inverse wave age, such that

$$\frac{z_o}{\sigma} = K(\frac{u_*}{C_p})^p \tag{9}$$

Drennan (2002) found best fit values of $K = 13.3$ and $p = 3.4$. These relationships will be evaluated in Section 5.

4 Data sets and flux computation

This study analyzes offshore tower and buoy data collected during six different field programs, each with unique geographical characteristics. The Risø Air Sea Experiment (RASEX) is described in Barthelmie et al. (1994) and Højstrup et al. (1995). In this study, we analyze observations taken at the sea mast west tower, located 2 km off the northwestern coast of the island of Lolland, Denmark, in 4 m of water, for the intensive observing period 3 October through 8 November 1994. The variation in mean water depth due to tides is only about 0.3 m. Local off-shore (southeasterly) flow is characterized by a sea fetch ranging between 2 km and 5 km. Sea fetch is the distance from land to the sea mast following the wind. On-shore flow has a sea fetch between 15 km and 25 km as it travels across an inland sea, and is still potentially fetch-limited in terms of wave age. Swell is less important compared to the other data sets. Fetch is the distance along the flow from the coast to the sea mast. Water depths for the longer fetches range from 4 m to 20 m. The nearby land surface is relatively flat. For additional characteristics of the instrumentation and flow regimes, see Mahrt et al. (2001b) and references therein. These data sets have been quality controlled using procedures similar to those in Vickers and Mahrt (1997a). In contrast to Vickers and Mahrt (1997b), we analyze the 6-m eddy correlation data instead of the 10 m data since the 6-m level is more suitable for thin stable boundary layers.

The largest data set analyzed here was collected from a 30 meter tower at the tip of a small very flat island (Östergarnsholm) approximately 4 km east of Gotland, Sweden. The footprint of the tower is over water with flow from the southerly sector. The bathymetry south of the island leads to minimal shoaling. Here, we analyze eddy correlation data collected at the 8-m level using a Gill Solent 101R2 sonic anemometer and wave data collected from a directional wave-rider buoy deployed approximately 4 km south of the site. This data contains a number of cases where the momentum flux was upward from the sea to the atmosphere. These cases are neglected in this study. Additional description of the instrumentation is detailed in Smedman et al. (1999).

We also analyze fluxes acquired by the Naval Postgraduate School's 'flux' buoy during two experiments conducted off the U.S. east coast. Both data sets are at approximately 5.25 m above mean sea level. During the first experiment, conducted in February-March of 1999, the buoy was located 10.5 km offshore of Duck, North Carolina, in 23 m of water. In the second

experiment, conducted in May-June 2000, the buoy was moored 13 km off Wallops Island, Virginia, in water 14 m deep. Unlike the two data sets previously described, which were obtained from stable towers, the NPS buoy measurements required motion corrections to remove wave motion-induced contamination from the observed wind data before eddy-correlation fluxes could be computed. High frequency 3-D wind and sonic temperature data were obtained from a Gill Instruments Model 1012/R3 ultrasonic anemometer mounted 5.25 m above the water surface. The buoy 3-D angular and linear motion data, used to perform motion corrections and to compute wave statistics, were obtained from a Systron-Donner MotionPak located within the buoy hull. The significant wave height was computed by summing the variance spectra for vertical displacement and multiplying by four. Further information on the NPS flux buoy instrumentation and data analysis procedures can be found in Frederickson and Davidson (2002).

After restrictions in subsection 4.1, the RASEX data set consists of 286 one-hour records, the NPS Wallops Island data set consists of 697 74-minute records, the NPS Duck data set consists of 313 48-minute records and the Östergarnsholm data set consists of 1142 one hour records.

For auxiliary analyses, additional data are extracted from Smith (1980) for open ocean conditions and SWADE data from Lake Ontario (Donelan et al. 1997). The data from Smith contains no cases of winds less than 4 ms^{-1} and is therefore listed only in Table 1. Since the SWADE data set is relatively small, we report values only for all wind speeds.

4.1   Data subsets

The influence of advection of turbulence from land appears to be confined primarily to the first 5 km downstream from the shore depending on wind speed and the upstream turbulence over land (Vickers et al., 2001). We require that the fetch is greater than 10 km. Because we pose no restrictions, such as minimum wind speed or flux magnitude, and because of the very large data sets, extreme values of the roughness lengths occur for some of the records. These extreme values can substantially influence attempts to fit the data with a model or compute bin-averaged values for different intervals of an independent variable. Therefore, we eliminate 5% of the outliers on both extremes of the frequency distribution of the roughness length.

9

4.2 Averaging

Due partly to random flux errors, the relationship between the roughness length and other variables is generally characterized by large scatter. Averaging the roughness lengths for a given interval of the independent variable can be strongly influenced by extreme values of the roughness length not excluded by the above criteria. With roughness lengths approaching zero, the log of the roughness length assumes very large negative values. As a result, logarithmically averaging roughness lengths lead to substantially smaller values of the roughness length compared to linearly averaging the roughness lengths. The frequency distribution of the log of the roughness lengths is approximately normal whereas the frequency distribution of the roughness length itself is strongly skewed toward positive values. In the latter case, averaging is not as well posed compared to normal distributions. An additional argument for logarithmic averaging is that the drag coefficient and stress depend on the natural logarithm of the roughness length. In subsequent sections, we will show results from both linear and logarithmic averaging.

4.3 Self-correlation

In general, the formulation of the roughness length in terms of other variables involving the friction velocity, heat flux and wind speed is influenced by self-correlation. Unless the variance explained by this self-correlation is estimated, it is not possible to determine from data if the formulation represents true inter-variable physical relationships. For example, the Charnock relationship relates the roughness length to the surface friction velocity; however, the roughness length is by definition a function of the surface friction velocity through the Monin-Obukhov relationship for the surface stress (Eq. 3). As a result, Smith et al. (1996) dismisses the Charnock relationship as a physically useful expression.

As one measure of the spurious self-correlation, we randomly redistribute the observed values of the friction velocity, heat flux, wind speed, wave phase speed and significant wave height. This process is carried out by assigning a record number to each of the N records for a given data set. The friction velocity for the first new random record is extracted from a record number chosen at random. This process is repeated independently for each variable until a new random record is determined. This process is repeated until a set of N new random records are constructed. For the N new random records,

we compute the roughness length from the randomized data for each of the N records and then compute the variance explained by the various roughness-length formulations. This entire process is repeated for 1,000 realizations and then the thousand values of the variance explained is averaged over all of the realizations. The procedure is applied to each of the data sets.

The variance explained by the original data less the variance explained by the randomized data is an estimate of the true physical variance explained. Since the randomized data may lead to very large absolute values of z/L, we impose the restriction $abs(z/L) < 2$ for both the original and randomized data. This restriction is applied only for this side study of self-correlation. The variance explained is based on the logarithm of the roughness length since the logarithm of the roughness length appears in the similarity prediction of the stress.

We have also examined the self-correlation by randomly specifying the values of wind speed, and heat and momentum fluxes according to a Gaussian distribution. While generally supporting results from the above "random redistribution" approach, the results based on the Gaussian noise approach depends on the assumption of normality. In this study, we report only results from the random redistribution approach.

5 Aerodynamic roughness length and Charnock coefficient

Even with near neutral conditions and large sea fetches, the Charnock coefficient for individual records varies by orders of magnitude partly due to the influence of wave age as well as random error. Based on studies in the literature as well as the present data sets, the Charnock coefficient generally:

1. decreases with wave age

2. increases at weak wind speeds with large scatter

3. is large for short sea fetch conditions (excluded from the present analysis) partly due to small wave age and advection of turbulence from land

4. is sometimes exceptionally small for stable conditions associated with warm air advection.

We temporarily remove weak wind cases ($U < 4ms^{-1}$) because the Charnock formulation is particularly poor for such conditions (Section 3). This condition removes many, but not all, of the ultra-smooth cases. Weak-wind cases will be restored at the end of this section. Except for large friction velocities, the logarithmic "average" value of the roughness length corresponds to a Charnock coefficient, which is smaller than in most previous data sets, partly because of the exclusion of weak wind cases and occurrence of a large number of records with wind following swell, discussed further in Section 6. The linear average of the roughness length corresponds to values of the Charnock coefficient, which are closer to previously published estimates (Figure 1). However, the average of the logarithm of the roughness lengths is much closer to a normal distribution and more suitable to averaging. For the combined data sets excluding the weak wind cases, the roughness length increases with u_*^2/g faster than linearly (Figure 1) so that corresponding Charnock coefficient increases with u_*^2/g.

Large scatter occurs in spite of self-correlation between the roughness length and friction velocity. This self-correlation is guaranteed by the definition of the roughness length (Eq. 3) and the definition of the drag coefficient. To investigate this self-correlation, we randomly re-arranged the observed values, as described in Section 4 and then computed the roughness length from the randomized data using Eq. 3. Based on these estimates, the physical variance explained (original variance minus that due to self-correlation) exceeds 20% only for the NPS-Duck data set (Table 1). Consequently, the variance explained by the Charnock relationship is usually dominated by spurious self-correlation. If the underlying physical correlation is of opposite sign to that introduced by self correlation, then the physical variance explained is negative and therefore not a true variance.
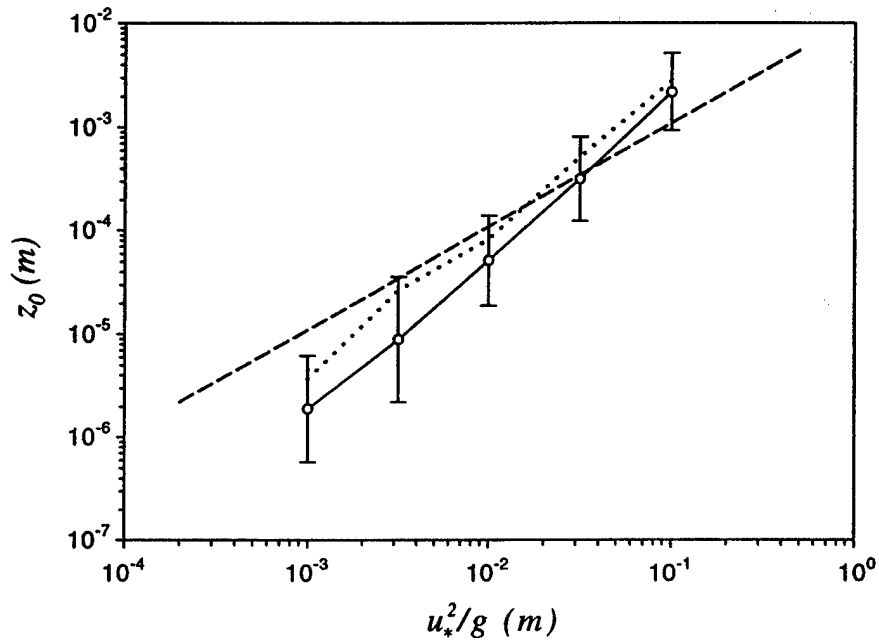
Figure 1: The dependence of the roughness length on u_*^2/g for all of the data sets combined using logarithmic averaging (solid line), excluding weak wind cases. The dotted line represents linear averaging. The dashed line is the Charnock prediction with $\alpha = 0.011$. The error bars indicate plus/minus one standard deviation. Standard errors would be extremely small because of the very large data set and would not be visible on the plot.

Table 1. Fraction of variance explained by various models for the aerodynamic roughness length: the Charnock formulation $z_o = \alpha u_*^2/g$ (char), the hyper model $z_o = (u_*^9/U^7)/g$ (hyper, Eq. 10), the wave age dependent model $z_o = (u_*/c_p)\alpha u_*^2/g$ (w.age, Eq. 7) and the wave height dependent model $z_o = \sigma_h(u_*/c_p)^3$ (w.height, Eq. 9). The desigation *orig* indicates the variance explained using the data sets listed in the first column. The designation *sim* indicates the variance explained after randomizing the data as described in Section 4. Weak winds ($U < 4ms^{-1}$) are excluded.

dataset	char orig	char sim	hyper orig	hyper sim	w.age orig	w.age sim	w.height orig	w.height sim
NPS-Duck	0.81	0.58	0.93	0.89	0.80	0.56	0.72	0.42
NPS-Wallops Is.	0.67	0.55	0.85	0.88	0.62	0.54	0.49	0.43
Öster.-8m	0.58	0.60	0.89	0.94	0.57	0.57	0.46	0.33
RASEX-6m	0.35	0.55	0.79	0.94	0.36	0.53	0.31	0.35
Smith1980	0.76	0.70	0.92	0.96	-	-	-	-

Table 2. Same as Table 2 except that weak winds are included.

dataset	char orig	char sim	hyper orig	hyper sim	w.age orig	w.age sim	w.height orig	w.height sim
NPS-Duck	0.67	0.55	0.91	0.88	0.66	0.53	0.62	0.40
NPS-Wallops Is.	0.17	0.43	0.55	0.85	0.16	0.42	0.14	0.35
Öster.-8m	0.38	0.51	0.82	0.92	0.37	0.49	0.29	0.31
RASEX-6m	0.25	0.52	0.67	0.92	0.24	0.51	0.20	0.37
SWADE	0.47	0.58	0.90	0.92				
SWADE-pure	0.85	0.69	0.98	0.97				

The Charnock coefficient increases with friction velocity probably because of the exponential dependence of the roughness length on u_*, embedded in the similarity relationship (Eq. 3) along with dependencies on wind speed and stability z/L. For neutral conditions, the roughness length and friction velocity are uniquely related for a given wind speed and observational height (Eq. 3). As an instructive example, we capitalize on this self-correlation and construct a two-parameter hyper-generalization of the Charnock relationship

of the form

$$\alpha \equiv \frac{z_o g}{u_*^2} = K^* (\frac{u_*}{U})^{p*}, \tag{10}$$

which allows for a higher order dependence of the roughness length on the friction velocity compared to the Charnock relationship. The constant coefficient K^* does not influence the variance explained. Rather large values of the exponent $p*$ provides the best fit. The second column in Table 1 lists the variance explained for $p*{=}7$. This relationship explains substantially more variance than the original Charnock relationship, approximately 90% (Table 1). However, within the error of estimating the self-correlation, the success of this model is due almost exclusively to self-correlation. This relationship simply captures even more spurious self-correlation than the original Charnock relationship.

One must also exercise care in interpreting the physical significance of additional parameters, which increase the order of the dependence of the roughness length on the friction velocity. For example, relating the roughness length to inverse wave age (Eq. 8) increases the dependence of the roughness length on the friction velocity by order p compared to the original Charnock formulation. For the wave-age dependent model ($p = 1$, column 3, Table 1), neither the total variance explained nor the variance explained by self-correlation increases significantly compared to the case of constant Charnock coefficient, even though relating the roughness length to inverse wave age is physically motivated by the expectation that growing young waves require more stress input than mature waves for a given wave amplitude.

The relative unimportance of wave age as an additional variable contrasts with Vickers and Mahrt (1997b) who found that the drag coefficient in RA-SEX, reduced to neutral, was significantly influenced by wave age. However, in their study, more stringent restrictions were placed on the allowed magnitude of z/L and cases with large random flux error were eliminated. These conditions reduce the scatter but create a bias in that they preferentially eliminate weak wind cases. They also included cases with sea fetch less than $10km$ where the wave-age effect is particularly strong. Johnson et al. (1998) show that the dependence of the Charnock coefficient on wave age becomes evident only when combining a variety of data sets in order to represent a sufficiently wide range of wave age.

Relating the roughness length scaled by the rms wave height to the inverse wave age (Eq. 9) explains substantially more physical variance only for the NPS-Duck data (fourth column, Table 1). Based on bin-averaged values
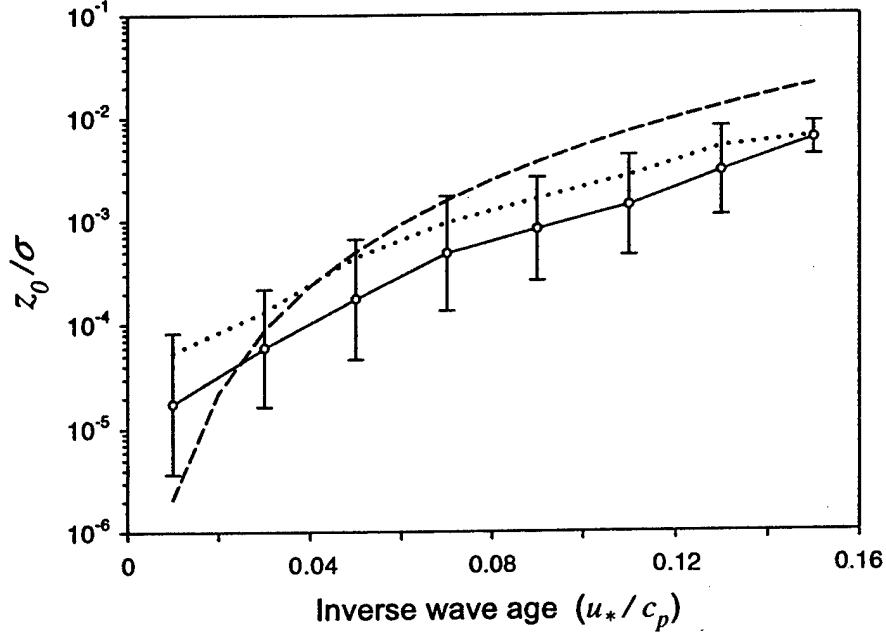
15

Figure 2: The dependence of the scaled roughness length on inverse wave age for all of the data sets, excluding weak wind cases. The dashed line presents the model in Drennan et al. (2002). The dotted line represents linear averaging.

for intervals of the inverse wave age, this model agrees with the trend found in the observations both in terms of the roughness length (Figure 2) and the Charnock coefficient (not shown). The magnitude of the scaled roughness length is generally smaller than that predicted by the model in Drennan et al. (2002), partly for reasons discussed above. On the other hand, using completely random data (Section 4), the bin-averaged nondimensional roughness length follows Eq. 9 reasonably well, although with a stronger dependence on inverse wave age, underscoring the role of self-correlation (also not shown).

Large self-correlation can be partly due to greater variation of the friction velocity compared to the wave phase speed. Drennan et al. (2002) reduces the impact of spurious self-correlation inherent with relating the roughness length to wave age, by seeking data with a wide range of wave phase velocities.

16

As in Drennan et al. (2002), we examine subsets of the data where the friction velocity is confined to a narrow interval, ensuring that the variation of wave age for the subset is due primarily to variation of wave phase speed. We found that partitioning data into intervals of friction velocity seriously reduced the variance explained by Eq. 9; that is Eq. 9 is affected by significant self-correlation for our data. Some of our data are significantly influenced by swell in spite of removal of weak wind cases. Drennan et al. (2002) carefully removed cases of significant swell.

If we include weak-wind cases, both the total variance explained and the variance explained due to self-correlation are substantially less for most of the data sets and models in this section (Table 2). For specification of constant Charnock coefficient, the total variance explained may be significantly less than that due to self-correlation. That is, for weak wind speeds, the Charnock formulation produces the wrong sign in the change of roughness length with wind speed and actually reduces the variance explained below the self-correlation value.

6   Ultra-smooth conditions

Often the roughness length computed from observations is smaller than that due to the smooth flow term, corresponding to ultra-smooth conditions (Donelan, 1990). For three of the four data sets, ultra-smooth cases, comprise a significant fraction of the cases; 38% for the NPS-Duck data, 49% for the Wallops Island data and 42% for the Östergarnsholm data. Only for the RASEX data are ultra-smooth conditions rare and the Charnock coefficient averages near the traditional value of 0.01. The RASEX data correspond to an inland sea and is the only data set with minimal swell.

Donelan (1990, p. 256) suggests that small differences between the wind and swell phase velocities could contribute to ultra-smooth conditions. Wind waves are thought to be suppressed with wind following the swell (Phillips and Banner, 1974; Mitsuyasu and Kusaba, 1996). The stress can decrease to arbitrarily small values, vanish and even reverse sign, corresponding to upward momentum flux from the sea to the atmosphere (Smedman, 1994; Grachev and Fairall, 2002 and references therein). When the swell-driven upward momentum flux approximately balances the downward wind driven momentum flux, the total stress is very small. For the data in Grachev and Fairall (2002), such conditions corresponded to winds between 1 and 2 ms^{-1},

17

although some influence of swell appeared to extend to stronger wind speeds.

For the Östergarnsholm data, wind following swell with near zero or upward momentum flux typically occurred with winds around 4 ms^{-1} (Smedman et al., 1999). For this data, the averaged Charnock coefficient is very small for winds between 4 ms^{-1} and 8 ms^{-1} (Figure 3). Here, the Charnock coefficient is defined without the smooth flow term and is based on winds transformed to 10-m values using Monin-Obukhov similarity theory. Again, linear averaging of the Charnock coefficient produces larger values (Figure 4).

The Charnock coefficient decreases to very small values for intermediate wind speeds for the Duck and Wallops Island data sets as well (Figure 3). For the swell-influenced data sets, the Charnock coefficient increases with increasing wind speed for winds greater than about 6 ms^{-1} and approaches more traditional values only for wind speeds greater than about 10 ms^{-1}, depending on the data set (Figure 3). The formulation with constant Charnock coefficient already implies a slow increase of roughness length with increasing wind speed (Section 3), but the observed roughness length increases faster than the rate predicted by constant Charnock coefficient.

After eliminating weak wind conditions, the Charnock coefficient systematically decreases with increasing wave age (C_p/U) for the Östergarnsholm data and the NPS Duck data (Figure 5). This is consistent with the notion that the very small values of the Charnock coefficient are often related to wind-following swell. The other two data sets did not show this relationship but did not contain an adequate sample of older wave ages for full examination of the dependence of the Charnock coefficient on wave age.

Is the dependence of the Charnock coefficient on wind speed related to a statistical relationship between wave age and wind speed? The increase of the Charnock coefficient with strong wind speeds is statistically due in part to a general decrease of wave age with stronger wind speeds and the decreased importance of swell at stronger wind speeds, as found in Oost et al. (2002) and Drennan et al. (2002). High wind events can be short term and the waves may not have time to reach near-equilibrium; that is, the phase speed of the waves remains small compared to the wind speed. Wave breaking may also play a role. For the RASEX data, the wave age does indeed systematically decrease with increasing wind speed (Vickers and Mahrt 1997b). For the data sets analyzed in this study, after excluding weak winds, the wave age also decreases with increasing wind speed. The correlation between wind speed and wave age for wind speeds greater than $6ms^{-1}$ are -0.6 for NPS-Duck,

18

-0.93 for NPS-Wallops Island, -0.45 for the Östergarnsholm data and -0.69 for the RASEX data.

The averaged Charnock coefficient is smallest for intermediate wind speeds because of the increase of the Charnock coefficient at stronger wind speeds and increase of the the Charnock coefficient at weak winds. Application of the smooth flow term reduces the Charnock coefficient, particularly at weak wind speeds (Figure 4), but significant increase of the Charnock coefficient at weak winds remains. Part of the increase of the Charnock coefficient at weak winds could be due to observational and analysis difficulties for weak wind speeds (Mahrt et al., 1996).

From a physical point of view, the Charnock formulation should not be applied to the present data sets where swell and young seas are common. However, most regional and large-scale models normally cannot accept the complexity of wave models. The correlation between the Charnock coefficient and wind speed suggests that the wind speed might be used as a statistical surrogate for the influence of wave state, even though such a surrogate would be physically indirect and incomplete. We avoid proposing such a formulation here since its generality would be unknown and the coefficients of such a formulation would be sensitive to the treatment of outliers.

7   Other influences

This analysis did not consider the direction of the swell. For swell opposing the wind, the drag coefficient is enhanced compared to pure wind-driven seas (Donelan et al., 1997). The swell propagation is often not aligned with the wind and the stress direction may be different from the wind direction. This invalidates Monin-Obukhov similarity theory, as emphasized in Grachev and Fairall (2002) and the roughness length and Charnock coefficient loose physical meaning. Rieder and Smith (1997) pose the change of the stress with wind speed by partitioning the stress into different frequency bands and separating the wave-coherent part of the stress. They find that differences between swell and wind direction, sometimes associated with nonstationarity of the wind field, can lead to wave-induced stress (eddies coherent with the wave field) that opposes the wind-induced stress. Coastal zone winds are frequently changing in time and space due to a diurnally varying component associated with thermal land-sea contrasts and SST variations as well as coastal advective effects. We are currently investigating the influence of swell
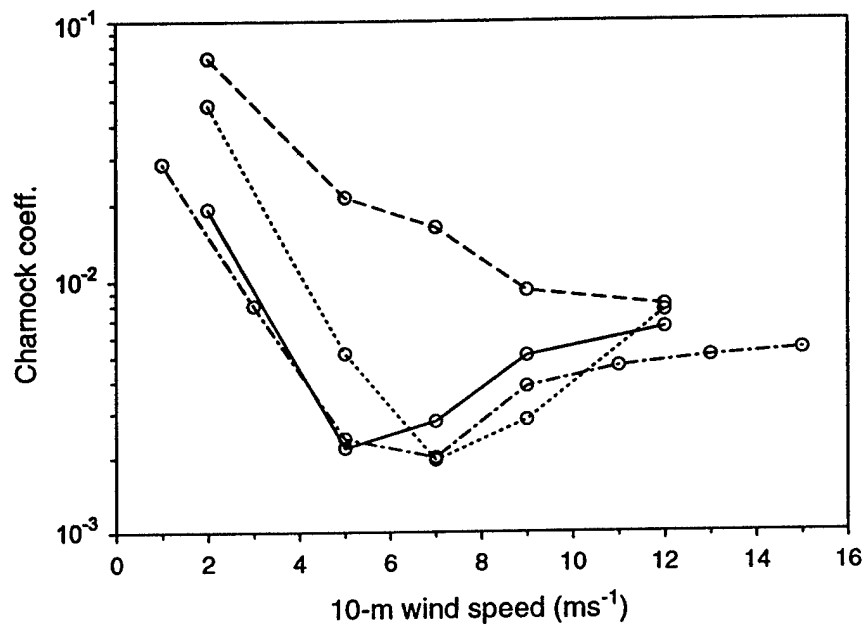
19

Figure 3: The dependence of the Charnock coefficient on wind speed for RA-SEX data (dashed line), Wallops Island data (dotted line), NPS-DUCK data (solid line) and Östergarnsholm data (dash-dotted) for logarithmic averaging. Values are several times larger for linear averaging.
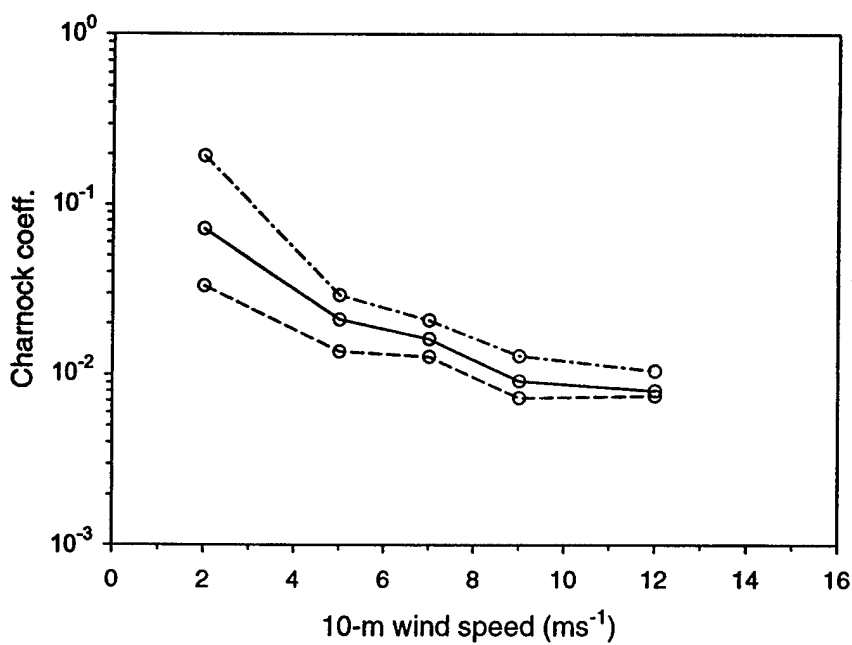
Figure 4: The dependence of the Charnock coefficient on wind speed for the RASEX data set for logarithmic averaging (solid line), linear averaging (dashed-dot) and logarithmic average with inclusion of the smooth flow term (dashed line).
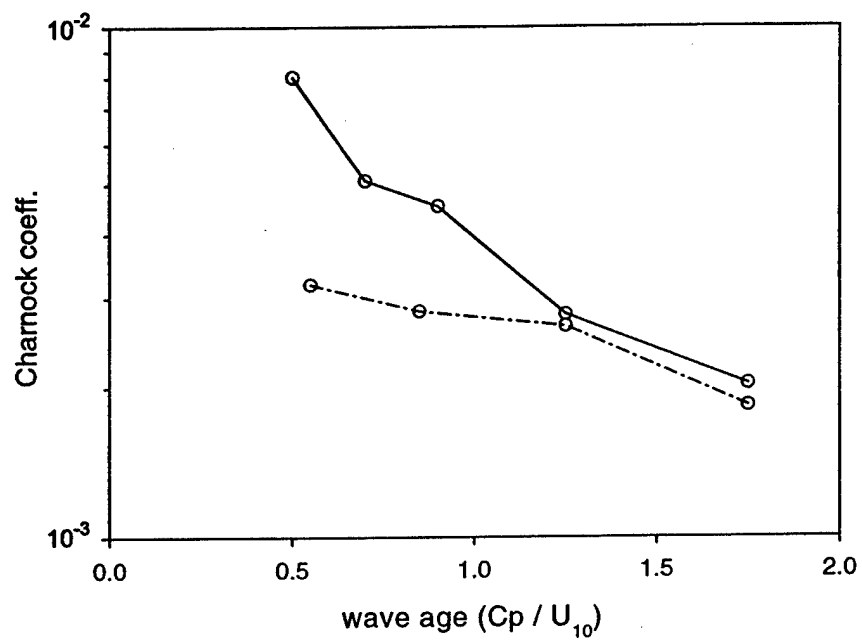
Figure 5: The dependence of the Charnock coefficient on wave age for the NPS Duck data (solid) and the Östergarnsholm data (dashed-dot).

direction.

Very small values of the stress also occur with strong stability (Smedman et al., 1997a, 1997b). Plant et al. (1998) and Mahrt et al. (2001a) have noted that the roughness length decreases with increasing stability. Stable stratification restricts turbulent transport to the wave surface, which can lead to further decrease of the roughness length and surface stress. As a possible result, the wave model examined by Voorrips et al. (1996) was found to over predict wave growth in stable conditions. The eddy correlation data analyzed in Mahrt (2001a) corresponds to decreasing Charnock coefficient with increasing stability. However, ultra-smooth conditions are not confined to very stable cases for the present data and stability appears to be a secondary influence.

8 Conclusions

For the data sets analyzed in this study, formulations for the aerodynamic roughness length based on the Charnock relationship and wave age are dominated by spurious self-correlation. Our goal was to assess the errors resulting from application of the Charnock relationship to a wide variety of conditions, as is done in many models. Most regional and large-scale models cannot accommodate the complexity and computer time required for a wave model. To construct such an assessment, we have not removed common cases of swell or other conditions where the Charnock relationship is not expected to apply.

The dominance of spurious self-correlation remains even after removing cases with short fetch, weak winds and upward momentum flux from the sea surface. In addition, the overall behavior of the Charnock coefficient is sensitive to the treatment of numerous outliers and the method for averaging over the various records. Relationships allowing the dependence of the Charnock coefficient on wave age are still dominated by self-correlation. Inclusion of information on the significant wave height modestly increases the physical variance explained. These assessments are based on linear correlation whereas the physical relationship between variables may be nonlinear.

The extreme variability of the Charnock coefficient is associated primarily with very small values, which appear to be related to wind following swell and, to a lesser extent, semi-collapsed turbulence in very stable conditions. For such conditions, the roughness length is less than the smooth flow pre-

diction; that is the stress is "ultra-smooth". For the RASEX data set, where swell is generally absent, ultra-smooth conditions are relatively rare. The Charnock coefficient decreases with increasing wave age, C_p/U, to values much below traditional values. For the present data sets, larger wave age more often occurs for intermediate wind speeds while younger waves more often occurs for stronger wind speeds. This introduces a statistical wind-speed dependence where the Charnock coefficient is small at intermediate wind speeds and increases with increaseing with wind speed. The Charnock coefficient also increases at weak wind speeds. Inclusion of smooth flow effects reduces but does not eliminate this increase at weak wind speeds.

The Charnock formulation should theoretically not be applied to weak wind conditions and conditions with significant influence of wave state where Monin-Obukhov similarity theory and the traditional concept of an aerodynamic roughness length break down. Nonetheless, formulations based on the Charnock coefficient will probably remain a primary parameterization for closing the surface stress in numerical models because simple alternatives do not exist. The present data sets suggest using a smaller value of the Charnock coefficient at intermediate wind speeds compared to traditional values of the Charnock coefficient, although the generality of this behavior is not known and a quantitative parameterization is not offered. The difference between the data sets in this study underscores the danger of developing process formulations based on an individual site.

Acknowledgments

References

Andreas, E., and K. Claffey, Air-Ice Drag Coefficients in the Western Weddell Sea. I. Values Deduced from Profile Measurements, *J. Geophys. Res.*, **100**, 4833-4843, 1995.

Barthelmie, R. J., M. S. Courtney, J. Højstrup, and P. Sanderhoff, The vindeby project: A description. Report R-741(EN), *Risø National Laboratory*, DK4000, Roskilde, Denmark, 1994.

Brutsaert, W. H., *Evaporation into the Atmosphere*, pp. 299, D. Reidel, Dordrecht, 1982.

Charnock, H., Wind stress over a water surface, *Quart. J. Roy. Met. Soc.*, **81**, 639-640, 1955.

Donelan, M. A., Air-sea interaction, in *Ocean Engineering Science*, edited by B. LeMehaute and D. M. Hanes, pp. 239-292, John Wiley and Sons, 1990.

Donelan, M. A., W. Drennan, and K. Katsaros, The air-sea momentum flux in conditions of wind sea and swell, *J. Phy. Oc.*, **27**, 2087-2099, 1997.

Drennan, W., H. Graber, D. Hauser, and C. Quentin, On the wave age dependence of wind stress over pure wind seas. Submitted to *J. Geophys. Res.*, 2002.

Dyer, A. J., A review of flux-profile relationships, *Boundary-Layer Meteorol.*, **7**, 363-372, 1974.

Edson, J. B. and C. W. Fairall, Similarity Relationships in the Marine Atmospheric Surface Layer for Terms in the TKE and Scalar Variance Budgets, *J. Atmos. Sci.*, **55**, 2311-2328, 1998.

Fairall, C. W., E. F. Bradley, D. P. Rogers, J. B. Edson, and G. S. Young, Bulk prameterization of air-sea fluxes for Tropical Ocean-Global Atmosphere Coupled-Ocean Atmosphere Response Experiment, *J. Geophys. Res.*, **101**, 3747-3764, 1996.

Frederickson, P. A., and K. L. Davidson, Observational buoy studies of coastal air-sea fluxes, To appear in *J. Climate*, 2002.

Geernaert, G. L., On modeling the wind stress direction based on thermal advection and surface waves, in *The Air-Sea Interface*, edited by Donelan, Hui and Plant, pp. 421-429, The Rosentiel School of Marine and Atmospheric Science, U. of Miami, USA, 1996.

Geernaert, G., Theory of air-sea momentum, heat and gas fluxes, in *Air-Sea Exchange: Physics, Chemistry and Dynamics*, edited by G. Geernaert, pp. 25-48, Kluwer, 1999.

Grachev, A. and C. Fairall, Upward momentum transfer in the marine boundary layer, *J. Phy. Oc.*, **31**, 1698-1711, 2001.

Hare, J. E., T. Hara, J. B. Edson, and J. M . Wilczak, A similarity analysis of the structure of airflow over surface waves, *J. Phy. Oc.*, **27**, 1018-1037, 1997.

Højstrup, J., J. Edson, J. Hare, M. S. Courtney, and P. Sanderhoff, The RASEX 1994 experiments. Risø-R-788, RisøNational Laboratory, Roskilde, Denmark (ISBN-87-550-2039-9), 1995.

Johnson, H. K., J. Høstrup, H. J. Vested, and S. E. Larsen, On the dependence of sea surface roughness on wind waves, *J. Phy. Oc.*, **28**, 1702-1716, 1998.

Maat, N., C. Kraan, and W. A. Oost, The roughness of wind waves, *Boundary-Layer Meteorol.*, **54**, 89-103, 1991.

Mahrt, L., D. Vickers, J. Howell, J. Edson, J. Hare, J. Højstrup, and J. Wilczak, Sea surface drag coefficients in RASEX, *J. Geo. Res., Oceans*, **101**, 14,327-14,335, 1996.

Mahrt, L., D. Vickers, J. Edson, J. Sun, J. Højstrup, J. Hare, and J. Wilczak, Heat flux in the coastal zone, *Boundary-Layer Meteorol.*, **86**, 421-446, 1998.

Mahrt, L., D. Vickers, J. Sun, T. Crawford, G. Crescenti, and P. Frederickson, Surface stress in offshore flow and quasi-frictional decoupling, *J. Geophys. Res.*, **106**, 20,629-20,639, 2001a.

Mahrt, L., D. Vickers, J. Edson, J. Wilczak, J. Hare, and J. Højstrup, Vertical structure of offshore flow during RASEX, *Boundary-Layer Meteorol.*, **100**, 47-61, 2001b.

Mitsuyasu, H. and T. Kusaba, The effect of swell on certain air-sea interaction phenomena, in *The Air-Sea Interface*, edited by Donelan, Hui and Plant, pp. 49-53, U. of Toronto Press, 1996.

Nordeng, T. E., On the wave age dependent drag coefficient and roughness length at sea, *J. Geophys. Res.*, **96**, 7167-7174, 1991.

Oost, W., G. Komen, C. Jacobs, and C. van Oort, New evidence for a relation between wind stress and wave age from measurements during ASGAMAGE, *Boundary-Layer Meteorol.*, **103**, 409-438, 2002.

Paulson, C. A., The mathematical representation of wind speed and temperature profiles in the unstable atmospheric surface layer, *J. Appl. Meteor.*, **9**, 857-861, 1970.

Phillips, O. M. and M. Banner, The effect of swell on the growth of wind waves, *J. Fluid Mech.*, **66**, 625-640, 1974.

Plant, W., W. Keller, V. Hesany, K. Hayes, K. Hoppel, and T. Blanc, Measurements of the marine boundary layer from an airship, *J. Atmos. Oceanic Tech.* , **15**, 1433-1458, 1998.

Rieder, K. F. and J. A. Smith, Removing wave effects from the wind stress vector, *J. Geophys. Res.*, **103**, 1363-1374, 1998.

Smedman, A.-S., M. Tjernström, and U. Hogström, The Near-neutral marine atmospheric boundary layer with no surface shearing stress: A case study, *J. Atmos. Sci.*, **51**, 3399-3411, 1994.

Smedman, A.-S., H. Bergström, and B. Grisogano, Evolution of stable internal boundary layers over a cold sea, *J. Geophys. Res.*, **102**, 1091-1099, 1997a.

Smedman, A.-S., U. Hogström, and H. Bergström, The turbulence regime of a very stable marine airflow with quasi-frictional decoupling, *J. Geophys. Res.*, *102*, 21,049-21,059, 1997b.

Smedman, A., U. Högström, H. Bergström, A. Rutgersson, K. Kalma, and H. Pettersson, A case-study of air-sea interaction during swell conditions, *J. Geophys. Res.*, **104**, 25,833-25,851, 1999.

Smith, S. D., Wind stress and heat flux over the ocean in gale force winds, *J. Phy. Oc.*, **10**, 709-726, 1980.

Smith, S. D., R. J. Anderson, W. A. Oost, C. Kraan, N. Maat, J. DeCosmo, K. B. Katsaros, K. L. Davidson, K. Bumke, L. Hasse, and H. M. Chadwick, Sea surface wind stress and drag coefficients: the HEXOS results, *Boundary-Layer Meteorol.*, **60**, 109-142, 1992.

Smith, S. D., F, W, Dobson, and R. J. Anderson, The wind stress-sea state relationship with mixed sea and swell, in *The Air-Sea Interface*, edited by Donelan, Hui and Plant, pp. 429-436, The Rosentiel School of Marine and Atmospheric Science, U. of Miami, USA, 1996.

Sun, J., D. Vandemark, L. Mahrt, D. Vickers, T. Crawford, and C. Vogel, Momentum Transfer over the Coastal Zone, *J. Geophys. Res.*, **106**, 12,437-12,448, 2001.

Toba, Y. and M. Koga, A parameter describing overall conditions of wave breaking, white capping, sea-spray production and wind stress, in Oceanic Whitecaps, edited by D. Reidel, E. C. Monahan and G. Mac Niocaill, pp. 37-47, 1986.

Vickers, D. and L. Mahrt, Quality control and flux sampling problems for tower and aircraft data, *J. Atm. and Oc. Tech.*, **14**, 512-526, 1997a.

Vickers, D. and L. Mahrt, Fetch limited drag coefficients, *Boundary-Layer Meteorol.*, **85**, 53-79, 1997b.

Vickers, D. and L. Mahrt, Observations of nondimensional shear in the coastal zone, *Quart. J. Roy. Met. Soc.*, **125**, 2685-2702, 1999.

Vickers, D, L. Mahrt, J. Sun, and T. Crawford, Structure of offshore flow, *Mon. Wea. Rev.*, **129**, 1251-1258, 2001.

Voorrips, A. C., V. K. Makin, and G. J Komen, The influence of stratification of the atmospheric boundary layer on wave growth, in *The Air-Sea Interface*, edited by Donelan, Hui and Plant, pp. 21-26, The Rosentiel School of Marine and Atmospheric Science, U. of Miami, USA, 1996.

Wilczak, J. M., J. Edson, J. Hojstrup, and T. Hara, The budget of turbulence kinetic energy in the marine atmosphere, in *Air-Sea Exchange: Physics, Chemistry and Dynamics*, edited by G. Geernaert, pp. 153-174, Kluwer, 1999.

Along-shore variations of offshore flow

Erin Moore

College of Oceanic and Atmospheric Sciences, Oregon State University, Corvallis, Oregon, USA

L. Mahrt

College of Oceanic and Atmospheric Sciences, Oregon State University, Corvallis, Oregon, USA

[1] Using eddy correlation data collected by the LongEZ research aircraft, the adjustment of atmospheric flow downstream from a coastline is examined. Along-shore variation of the turbulence over the water is generated by the varying width of the upstream land strip between the sea and inland water. Over the coastal zone, the turbulence is strongest downstream from the widest part of land. The along-shore variation of the turbulence decreases with increasing sea fetch due to horizontal mixing. In other terms, the footprint of the flux farther offshore includes a larger width of upstream land. Beyond 5 km sea fetch, the along-shore variation becomes small.   *INDEX TERMS:* 0312 Atmospheric Composition and Structure: Air/sea constituent fluxes (3339, 4504); 3307 Meteorology and Atmospheric Dynamics: Boundary layer processes; 3329 Meteorology and Atmospheric Dynamics: Mesoscale meteorology; 3379 Meteorology and Atmospheric Dynamics: Turbulence. **Citation:** Moore, E., and L. Mahrt, Along-shore variations of offshore flow, *Geophys. Res. Lett.*, *30*(3), 1109, doi:10.1029/2002GL016240, 2003.

1. Introduction

[2] Boundary-layer adjustment in offshore flow may vary along the coast due to heterogeneity of the upstream land surface. *Winstead and Mourad* [2000] and *Winstead and Young* [2000] used synthetic aperture radar (SAR) imagery to show a connection between upstream variations of land surface and signatures over the water in offshore flow. In the present study, aircraft data are used to examine a similar connection between the width of land between inland water and the sea (Figure 1) and the turbulence measured downstream over the sea. Flow from the inland water over the land leads to development of a convective internal boundary layer due to heating over the warmer land surface and due to greater roughness over the land compared to the upstream water. The convective boundary-layer is expected to be deeper and more turbulent where the land is wider. The 1–5 km variation of land width is thought to influence flow more strongly than the modest along-shore variations of the land roughness and surface heating although quantitative assessment from the data is not possible.

2. Data

[3] This study analyzes data taken on and off the coast of the Outer Banks, North Carolina, USA. The Outer Banks is a narrow strip of land between the Abermarle Sound and the Atlantic Ocean (Figure 1). The Outer Banks ranges from about 1 to 5 km in width in the region of the aircraft flights. The Shoaling Wave Experiment (SHOWEX) took place during 26 October-12 November 1997, 2–18 March 1999, and 11 November-5 December 1999. The LongEZ (N3R) aircraft is equipped with a Best Aircraft Turbulence (BAT) probe, which measures the mean and turbulent wind fields. These data were collected at 50 samples per second, at approximately 55 ms^{-1} airspeed, which corresponds to a sample interval of about 1 m.

[4] Further description of the flights and data can be found in *Crescenti et al.* [1999], *French et al.* [2000] and *Sun et al.* [2001]. This study focusses on repeated flight tracks parallel to the coast at varying heights above the surface and distances from shore. We emphasize 4 Dec. 1999, which included the most extensive spatial coverage near the surface in offshore flow over the coastal zone. On this day, parallel flight tracks were flown at 1, 2, 4, 8, and 16 km offshore.

[5] The lowest flight levels were approximately 10 m above the sea surface, the highest were about 300 m. Flights parallel to the shore are used in an attempt to ensure an approximately constant sea fetch. However, small variations in sea fetch can be important for flight tracks closest to the coast, which probably contributes to the scatter in relationships examined in the next section. Data are selected with wind directions of 190–310 degrees to ensure offshore flow.

[6] To examine the influence of advection of turbulence from land on the structure of the offshore flow, the data are separated into classes of near shore (less than 2 km sea fetch), mid-distance (2–5 km sea fetch) and far shore (5–16 km sea fetch). To estimate the vertical structure of the flow, the data are also separated into low-level (<30 m), mid-level (30 m < z < 250 m) and high-level (>250 m) classes. To examine the along-shore variation, the flight tracks parallel to the shore are segmented into 2 km sections. These procedures partition the atmospheric boundary layer in the coastal zone into cubes. All of the turbulence quantities amongst the different aircraft passes, which fall into a given cube for a given flight, are aggregated into one value in order to reduce flux sampling errors. Even with such averaging, random sampling errors for turbulence quantities are estimated to remain significant. For 4 Dec. 1999, this aggregation includes 4 passes for each of the low-level cubes.

[7] The friction velocity at any level is computed as

$$u_* = \left(\left(\overline{w'u'} \right)^2 + \left(\overline{w'v'} \right)^2 \right)^{0.25} \tag{1}$$

and the drag coefficient is defined as

$$c_D = \frac{u_*^2}{U^2} \tag{2}$$
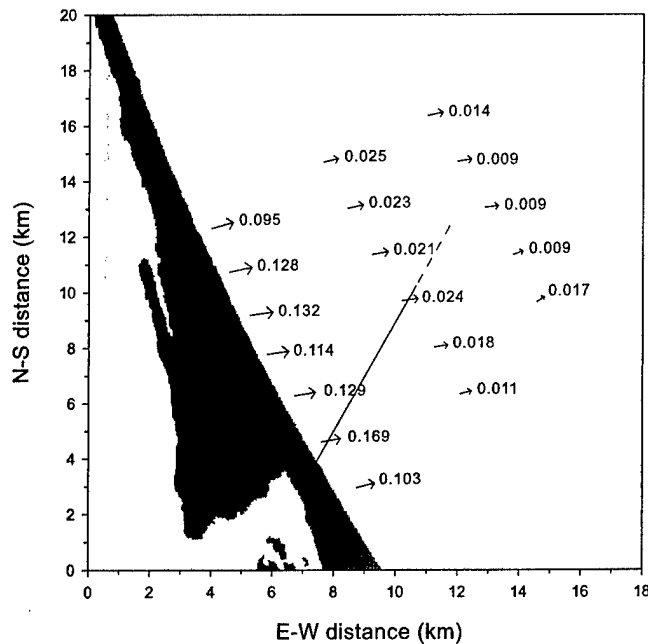
Figure 1. The spatial distribution of the vertical velocity variance, $\overline{w'w'}$, and wind vectors over the coastal zone for flight levels below 30 m. The sketched line depicts the northward shift of the maximum vertical velocity variance with increasing offshore distance.
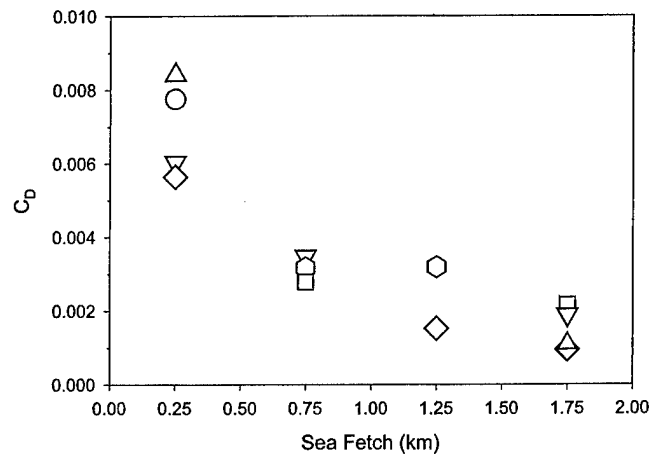
Figure 2. c_D as a function of sea fetch, $z < 30$ m, sea fetch <2 km, for 6 study days. Flight dates with (z/L) values in parentheses are: square = 4 March 1999 (-0.077); upside down triangle = 16 March 1999 (0.107); triangle = 18 March 1999 (0.289); $\circ$ = 2 Nov. 1997 (0.001); pentagons = 9 Nov. 1997 (-0.151); $\diamond$ = 4 Dec. 1999 (0.053).

where primes denote fluctuations from an unweighted 1-km mean, overbars symbolize 2-km averages, and U is the wind speed computed from averaged wind components. The 1-km average is chosen to reduce contamination of the perturbation flow by mesoscale motions while the 2-km average of the flux is chosen to reduce flux sampling errors. For aircraft levels above the surface layer, the drag coefficient, c_D, would not satisfy Monin-Obukhov similarity theory.

3. Along-Shore Spatial Variations of Offshore Flow

[8] The drag coefficient and other turbulence quantities decrease rapidly with offshore distance (sea fetch) due to the decreasing roughness and formation of stable stratification (Figure 2), as examined in *Vickers et al.* [2001] and *Sun et al.* [2001]. The scatter is partly due to different atmospheric stability and different upstream land fetch. The turbulence decreases faster downstream from the coast in stable conditions (warm air over cold water) due to buoyancy destruction of the turbulence.

[9] Close to shore, the vertical velocity variance for the low-level flights is substantially larger downstream from wider land width (Figure 1). A secondary maximum of vertical velocity variance occurs farther north perhaps due to a small forest over the upstream land.

[10] Farther offshore from the widest part of the land, the footprint of the flux begins to include more of the narrower southerly land region. This causes the location of maximum vertical velocity variance to shift farther north, as shown by the sketched line in Figure 1. This process is schematically depicted in Figure 3, where the upstream footprint of the flux incorporates a larger north-south segment of the coast with increasing offshore distance. The footprint spatially

integrates the land influence so as to not show a sharp maximum farther offshore. Numerical application of footprint theory (e.g., *Horst and Weil*, 1994) is not attempted since the flow is in a state of rapid adjustment induced by the discontinuity in surface conditions. The along-shore variation fades with further increase of sea fetch and the north-south maximum of the vertical velocity variance for flight tracks greater than 5 km offshore becomes ambiguous (Figure 2). At higher flight levels, along-shore variation of the turbulence offshore is also evident, but the data sample is smaller than that for the low-level data. A similar pattern
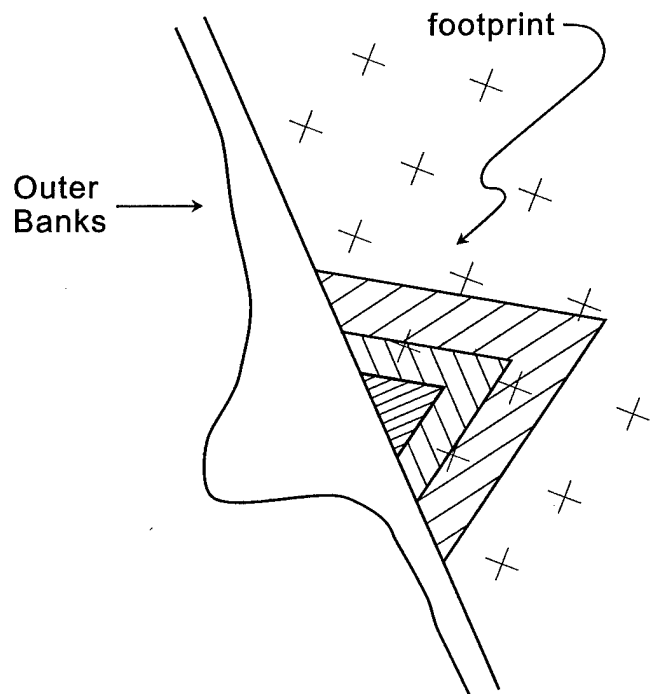
Figure 3. Schematic of the land footprint captured in the flux measurements for different distances offshore.

occurred on other flight days but was noisier, probably due to the smaller sample of turbulence data at a given point.

4. Conclusions

[11] The variable width of the upstream land, separating the open ocean from inland water, induces along-shore variation of the sea-surface stress with offshore flow, particularly in the first few kilometers offshore. The influence of spatial variations of heat flux and surface roughness over the land could not be quantitatively assessed. Future examination of offshore flow structure should include more days to examine different boundary-layer situations and a larger number of passes over a given point in order to accumulate a larger sample size for resolving the spatial variation of the turbulence quantities.

References

Crescenti, G. H., T. L. Crawford, and E. J. Dumas, Data Report: LongEZ (N3R) Participation in the 999 Shoaling Waves Experiment (SHOWEX) Spring Pilot Study, NOAA Technical Memorandum ERL ARL-232, Silver Spring, MD, 86 pp., 1999.

French, J. R., G. H. Crescenti, T. L. Crawford, and E. J. Dumas, LongEZ (N3R) Participation in the 999 Shoaling Waves Experiment (SHOWEX), NOAA Data Report OAR ARL-20, Silver Spring, MD, 51 pp., 2000.

Horst, T. W., and J. C. Weil, How far is far enough?: The fetch requirements for micrometeorological measurement of surface fluxes, *J. Atmos. Oceanic Technol., 11*, 1018–1025, 1994.

Sun, J., D. Vandemark, L. Mahrt, D. Vickers, T. Crawford, and C. Vogel, Momentum transfer over the coastal zone, *J. Geophys. Res., 106*(12), 437-12, 488, 2001.

Vickers, D., L. Mahrt, J. Sun, and T. Crawford, Structure of Offshore Flow, *Mon. Wea. Rev., 129*, 1251–1258, 2001.

Winstead, N. S., and P. D. Mourad, Shallow Great Lake-Scale Atmospheric Thermal Circulation Imaged by Synthetic Aperture Radar, *Mon. Wea. Rev, 128*, 3654–3663, 2000.

Winstead, N. S., and G. S. Young, An analysis of exit flow drainage jets over the Chesapeake Bay, *J. Appl. Meteorol., 39*, 1269–1281, 2000.

L. Mahrt and E. Moore, College of Oceanic and Atmospheric Sciences, Oregon State University, 104 Ocean Admin Bldg, Corvallis, OR 97331-5503, USA. (mahrt@coas.oregonstate.edu)

FLOW ADJUSTMENTS ACROSS SEA-SURFACE TEMPERATURE CHANGES

L. MAHRT (mahrt@coas.oregonstate.edu), DEAN VICKERS and
ERIN MOORE
*College of Oceanic and Atmospheric Sciences, Oregon State University, Corvallis,
OR 97331, U.S.A.*

Abstract. The adjustment of airflow across sea-surface temperature changes is examined using aircraft eddy-correlation data. Major features of the observed flow adjustment are not included in the theory of internal boundary layers. However, the data sample size and coverage are not sufficient to accurately quantify the additional influences. With flow from warm water over cooler water, substantial turbulence intermittently develops above the newly formed surface inversion layer. The corresponding, spatially-averaged, downward momentum flux is stronger than that close to the surface.

With stably stratified flow over modest increases of sea-surface temperature, reduction of stratification can trigger episodic shear generation of turbulence. In these cases, the primary role of increasing surface temperature in the downwind direction is to induce shear generation of turbulence. With larger increases of surface temperature, upward heat flux generates turbulence, warms the air and generates a significant horizontal gradient of hydrostatic pressure. This contribution to the pressure field appears to strongly modify the flow. Major inadequacies in existing data and future needs are noted.

Keywords: Internal boundary layer, SST front, Heterogeneity, Secondary circulations, Mesoscale

1. Introduction

Airflow over a surface temperature discontinuity often induces an internal boundary layer as the air near the surface adjusts to the new surface conditions. Unstable internal boundary layers, as with flow of cool air over warm water, have been studied in detail and are reasonably well understood, particularly on the mesoscale where the internal boundary layer is capped by an inversion or entrainment zone (e.g., Steyn and Oke, 1982; Garratt, 1990; Attié and Durand, 2003). On smaller horizontal scales where such a capping inversion is not yet formed, the top of the internal boundary layer can be defined in terms of the top of bent over thermals rising into cooler air (Mahrt, 2000; Klipp and Mahrt, 2003). In this region just downwind from the surface temperature increase, the vertical transfer may still be influenced by upwind dynamics (Andreas and Cash, 1999).

Stable internal boundary layers forming in flow of warm air over cooler surfaces are even more complex and less understood (Garratt, 1987; Vickers et al., 2001; Sun et al., 2001). The stable internal boundary layer can be difficult to define in terms of turbulence structure, since the turbulence often increases with height and reaches a maximum above the surface stable layer (Mahrt 2000). The decoupled flow above the surface stable layer accelerates and a low-level wind maximum, similar to the nocturnal jet, may form (Smedman et al., 1995; Vihma and Brümmer, 2002).

The present study analyzes aircraft eddy correlation data collected in flow over changes of sea surface temperature. A number of important features are identified, which are not included in the above studies. For example, small increases of surface temperature in the downwind direction can lead to thermally-induced shear generation of turbulence without development of a convective boundary layer (Section 3.1). The local pressure gradient associated with the horizontal temperature gradient can strongly alter the flow (Section 3.2). With decrease of surface temperature and formation of a stable surface inversion layer, significant turbulence intermittently develops above the surface inversion layer (Section 4). Inadequacies of the present data and future needs are outlined in Section 5.

2. Data

This study analyzes data taken off the coast of the Outer Banks of North Carolina, USA during the Shoaling Wave Experiment (SHOWEX; Crescenti et al., 1999, French et al., 2000 and Sun et al., 2001) conducted 11 November-5 December 1999. Here we analyze data collected by the LongEZ (N3R) aircraft, including the three wind components, temperature and humidity at a rate of 50 samples per second. With an approximate air speed of 55 m s^{-1}, this sampling rate corresponds to a sample width of about 1 m.

Three flights were carried out perpendicular to shore about 100 km east of the coast over the western edge of the Gulf Stream. Passes were flown at two levels in the lowest 100 m and supplemented with aircraft soundings. The western edge of the Gulf Stream was locally directed more or less parallel to the coast (approximately south southwest to north northeast) during the flights. The sea-surface temperature (SST) increases by typically 4 °C across the western boundary of the Gulf Stream (Figure 1). On 19 November, when the air flow was approximately parallel to the SST front, the front is particularly sharp (Figure 1). On 20 November with a westerly wind component across the Gulf
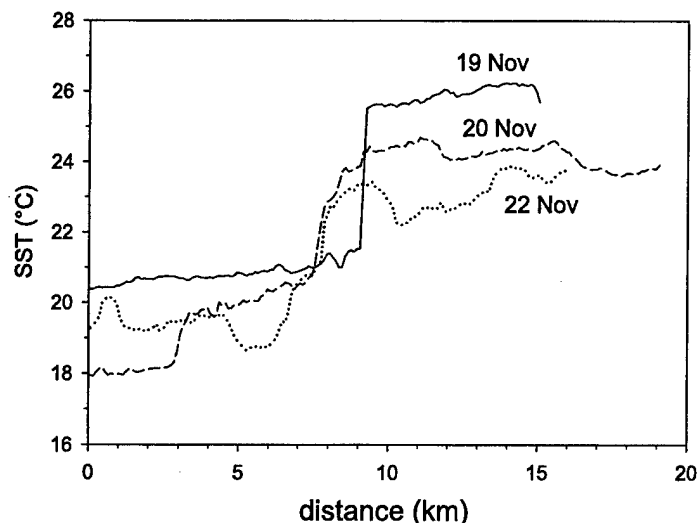
Figure 1. The horizontal variation of the SST across the western edge of the Gulf Stream along the east-west flight track on 19, 20 and 22 November.

Stream, the SST front is not as sharp and a secondary SST front is located about 5 km west of the main front with a temperature increase of about 1.5 °C (Figure 1). This secondary front occurs as a local temperature maximum when viewed from the 8-m flight track instead of the 33-m flight level, which was slightly displaced horizontally from the track at 33 m. On 22 November, the wind is easterly and the SST front is not very sharp with multiple small-scale variations.

Air-sea temperature differences are expressed in terms of a local potential temperature $(\mathrm{T(z)} + 0.01\ z\ °\mathrm{K\ m}^{-1})$, where z is the aircraft altitude above the sea surface in metres. Unfortunately, the radiometrically-measured sea-surface temperature is not very accurate due to drift of the reference temperature of the Everest Interscience Inc. 4000.4GL. Absolute errors may be as large as 1°C. Therefore, the radiometer measurements will be used only to qualitatively determine the spatial pattern of the sea-surface temperature.

Order of magnitude estimates of the buoyancy and shear generation of turbulence energy will be made. The shear generation of turbulence can be expressed as

$$\frac{u_*^3 \phi_m}{\kappa z} \tag{1}$$

where ϕ_m is the nondimensional shear, estimated as a function of z/L from Monin-Obukhov similarity theory. The fluxes and the friction velocity have been estimated from the eddy correlation measurements

using a 2-km averaging window. The friction velocity is computed from both the along-wind and cross-wind components as is the magnitude of the momentum flux used in the Obukhov length. Fluxes at the aircraft level may be different than the surface values, particularly for stable conditions. While similarity theory may be only a crude approximation, we believe it to be more accurate than estimating the actual shear near the surface using winds from the two aircraft levels.

3. Flow from cool to warmer water

3.1. Upwind from the SST front

On 20 November, southwesterly flow of cooler air over the warmer water leads to development of a convective internal boundary layer. Based on profiles of potential temperature and moisture provided by an aircraft sounding upwind from the SST front near the west end of the aircraft track, the depth of the stable inversion layer is about 70 m. The turbulence upwind from the SST front near the surface (8-m level) is relatively weak (Figure 2, lower panel). The friction velocity is typically between 0.05 and 0.10 m s^{-1}. At the 33-m level, the turbulence is even weaker (Figure 2, upper panel) and the friction velocity is typically about 0.02 m s^{-1}, considered to be zero within observational error. These values suggest a thin turbulent boundary layer, shallower than 30 m and significantly shallower than the surface inversion layer. The depth of the surface inversion layer was well defined in terms of vertical profiles of the potential temperature and specific humidity constructed from aircraft slant soundings.

The data at 8 m show patches of enhanced turbulence, sometimes associated with small local increases of the SST upwind from the main SST front. Generally this local enhancement of turbulence is associated with an increase of momentum flux without observable upward heat flux. The example record in Figure 3 shows three types of turbulence events. With the first type, significant turbulence and downward momentum and downward heat flux develop at the 10-km location (Figure 3) without any SST change. This type of event did not occur with this strength in the other records. In the second type of turbulence event, very weak upward heat flux and increase of turbulence occur at a horizontal distance of 17 km (Figure 3) where the SST increases by about 1° C. Significant turbulence but no upward heat flux develops at 22 and 25 km (Figure 3), where the SST gradually increases just west of the main SST front. Upward heat flux develops just downwind from this event.

Considering all five records at the 8-m level upwind from the main SST front, eight events were defined where u_* locally exceeds 0.1 m s^{-1}. Five of these events were associated with an increase of SST of about 1 °C or greater. Since the SST increases occupy a small fraction of the flight path, we conclude that locations of SST increases are preferred locations for turbulence development. For four of the five events, buoyancy generation of turbulence was negligible or at least an order of magnitude smaller than the shear generation of turbulence. In the other case, the buoyancy generation was as large as the shear generation. For cases of turbulence development without upward heat flux, the turbulence could be generated by shear instability induced by reduction of the positive air-sea temperature difference and corresponding reduction of the bulk Richardson number. Since the air temperature changes much more slowly than the sea-surface temperature, small-scale changes of the air-sea temperature differences track closely with small-scale changes of the sea-surface temperature. While these observations are suggestive of the importance of thermally-induced shear generation, the number of events is far too small to form definite conclusions.

For three of the five passes at the 33-m level, the increased turbulence upwind from the main SST front leads to local cooling of the air of about 0.5 °C (e.g., Figure 2, 10 km point, upper panel). This cooling is presumably due to mixing of cooler air from near the surface upward to the aircraft level.

3.2. THERMALLY-INDUCED PRESSURE GRADIENT

The heat flux downwind from the SST front is usually upward but does not become strong at the aircraft level until several kilometers further downwind (Figure 4). The increase of heat flux on this day lags the increase of momentum flux by several km at the 33-m flight level (Figure 4), with considerable variability between passes. As a result, the turbulence in the airflow immediately downwind from the main SST front is generated primarily by shear. This could correspond to the "mixed" regime reported by Andreas and Cash (1999) where the upwind dynamics still influences the vertical transfer immediately downwind from a surface temperature increase. The buoyancy generation could act more as a catalyst for strong shear generation of turbulence. As the flow moves farther downwind from the SST front over the warmer sea surface, the convective turbulence strengthens and deepens.

The warming of the air over the warmer water leads to a significant horizontal temperature gradient over the first 5 km downwind from
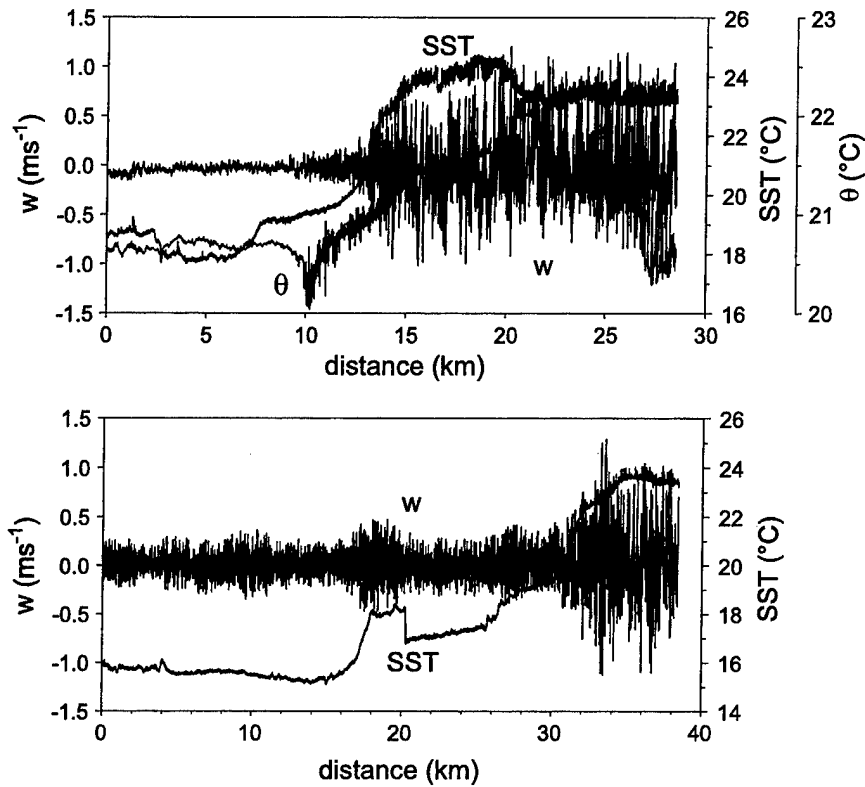
Figure 2. The horizontal variation of SST, air potential temperature (θ on an expanded vertical scale) and vertical velocity (w) for an individual pass at 33 m (upper panel) and an individual pass at 8 m (lower panel) on 20 November. The flow is from left to right.

the SST front (Figure 5, upper panel). The westerly flow component accelerates across the region of strong horizontal temperature gradient toward the warmer air (Figure 5, 8-14 km). Such horizontal acceleration is consistent with a local horizontal pressure gradient due to horizontal variation of the air temperature. This contribution to the pressure field corresponds to lowest surface pressure under the warmest air. That is, we hypothesize a thermal low pressure system, which is superimposed on the larger-scale pressure gradient.

Using the sounding data together with the two horizontal flight levels, the thermally-induced pressure gradient along the flight track was estimated by vertically integrating the hypsometric equation between the surface and the 100-m level, the perceived maximum depth of significant horizontal temperature variation. The height dependence
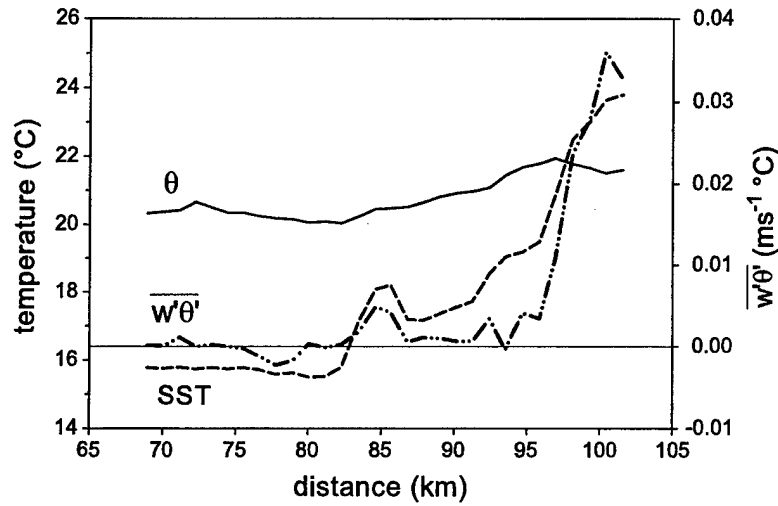
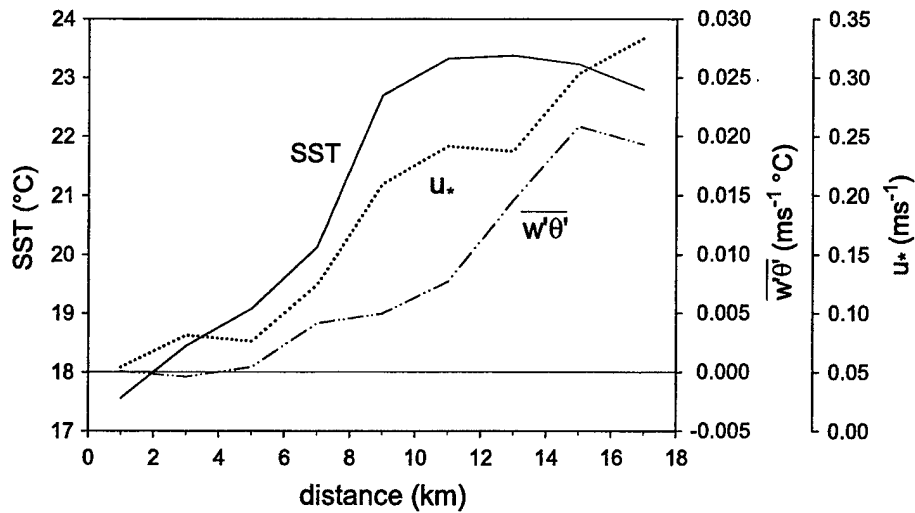*Figure 3.* An example of 1-km fluxes for a single pass at 8 m on 20 November.

Figure 4. The spatial variation of the SST, friction velocity and heat flux at 33 m near the main SST front on 20 November. The values are composited over the 5 passes. The compositing causes some spatial spreading because the individual records are not perfectly aligned with respect to the SST front. The flow is from left to right.
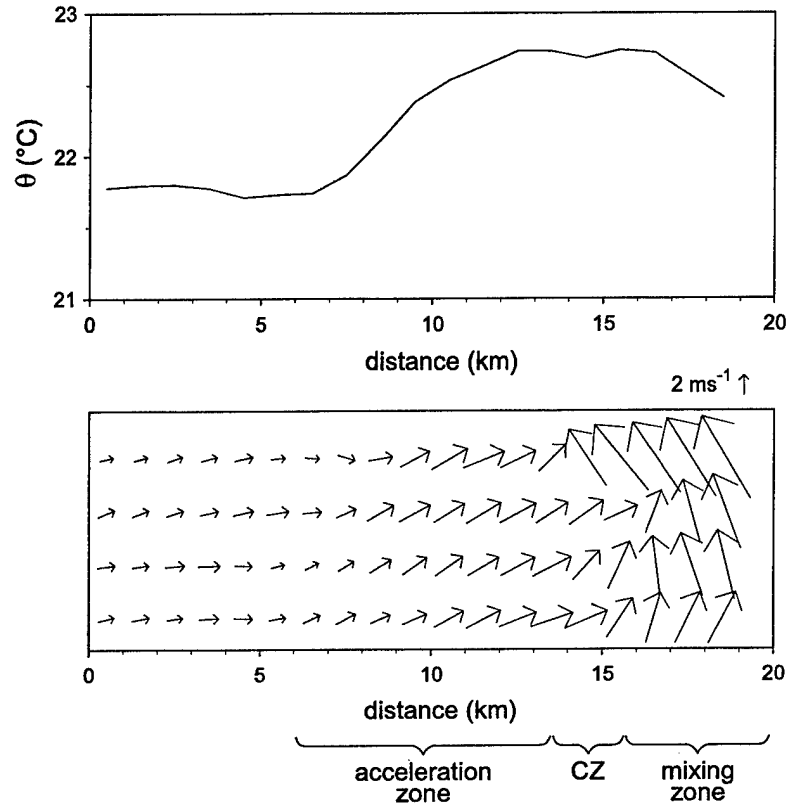
Figure 5. The along-flight variation of the composited potential temperature at the 33-m level on 20 November (upper panel) and the 1-km averaged wind vectors at 33 m (lower panel) for 4 sequential passes over the same track, the first pass is at the top and so forth. A unit vector of 2 m s $^{-1}$ is shown above the right hand corner. The vectors are plotted as a planview with north directed upward and east directed to the right. The bracketing delineates the zone where the flow is accelerated toward the warmest air, the convergence zone (*CZ*) and the zone where strong southerly momentum is convectively mixed downward toward the surface.

of the horizontal temperature gradient was fit to an exponentially decaying function with the amplitude based on the lowest flight level and a decay height of 100 m. The thermally-induced pressure gradient is also estimated with a simpler approach (Equation 9 in Mahrt, 1982) of the form

$$\frac{g}{\Theta}h\frac{\partial[\theta]}{\partial x},\qquad(2)$$

where $[\theta]$ is the vertically integrated potential temperature from the surface up to a constant depth, h, and Θ is a scale value of the poten-

tial temperature. The vertically- and horizontally-averaged potential temperature for both sides of the SST front were determined from both aircraft levels and the aircraft soundings. The order of magnitude of the thermally-induced pressure gradient determined by the two methods is estimated to be between 10^{-4} and 10^{-3} m s $^{-2}$. The magnitude of the Coriolis term near the surface in the acceleration zone (Figure 5) is approximately 4×10^{-4} m s^{-2}. The magnitude of the large-scale pressure gradient term is estimated by assuming that the southerly flow above the surface flow is approximately geostrophic. The value of the large-scale pressure gradient term is then estimated to be about 8×10^{-4} m s^{-2}. The other terms in the momentum budget could not be estimated with adequate accuracy to form even order of magnitude estimates. These calculations indicate that the thermally-induced horizontal pressure gradient is important. However, errors in the estimation of the thermally-induced pressure gradient are probably large because of limited information on the vertical structure over the warm side of the SST front. However, the sign of the thermally-induced horizontal pressure gradient near the surface is consistent with acceleration of the westerly flow component across the region of large horizontal temperature gradient.

The southerly flow observed at the surface east of the convergence zone (Figure 5) is probably due to strong downward mixing of stronger southerly flow. This strong downward mixing is caused by the buoyancy-driven turbulence. The aircraft soundings show stronger southerly flow at higher levels over the entire region, presumably driven by the large-scale pressure gradient. This downward mixing does not eliminate the westerly flow near the surface in the region of strong horizontal temperature gradient (acceleration zone, Figure 5). Apparently, west of the convergence zone but still over the warm water, the local thermally-induced horizontal pressure gradient is more important than the downward mixing of momentum.

4. Stable case

A stable inversion layer develops on 22 November when easterly flow advects warm air from over the warmer water to over the cooler water. The generally weak upward heat flux over the warmer surface on this day changes to weak downward heat flux downwind from the SST front over cooler water. The magnitude of the downward momentum flux at the 9-m flight level decreases downwind over the cooler water accompanied by considerable modulation.
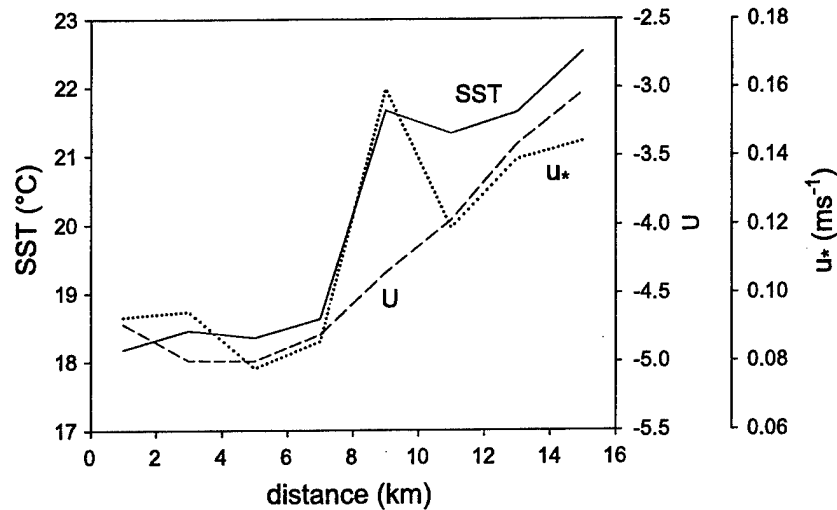
Figure 6. The spatial variation of 2-km averages of SST, u_* and the westerly wind component (U), here negative, for flow from warm water over cooler water on 22 November for the 9-m flight level. Values have been composited over 6 passes. The flow is from right to left.

The spiral aircraft sounding taken over the cool water shows a surface stable layer forming downwind of the SST front up to about 50 m above the surface at the sounding location. A warmer residual layer overrides the stable surface layer and extends from 50 m up to about 300 m above the surface. At the 90-m flight level within the residual layer, the turbulence decays rapidly downwind from the SST front, but dramatically increases at a patch of turbulence about 2 km wide for each of the two passes. The events are characterized by large u_* values, exceeding 0.3 m s $^{-1}$. For the single pass at 280 m, a similar turbulent burst is observed. The bursts occur at different relative positions with respect to the main SST front and do not seem related to variations of SST downwind from the main front. They are apparently driven by shear above the surface inversion. As a result of these events, the spatially-averaged turbulence energy and momentum flux are larger at the 90-m level than at the 9-m level, albeit, random flux errors are large. Since the turbulence and stress increase with height, the turbulence is no longer surface-based in the sense that the primary source of turbulence is at higher levels. Based on aircraft data across an open ocean sea-surface temperature front, Friehe et al. (1991) found that the stress decreased with height even on the stable side over the

cooler water, although the SST front was weaker than in the present study.

5. Conclusions and discussion

With flow of warm air over cooler water, relatively strong intermittent bursts of downward transport of momentum occur above the newly formed surface inversion over the cooler water. As a result, the magnitude of the spatially-averaged downward momentum flux increases with height, although flux sampling errors are large.

With modest increases of surface temperature, significant turbulence and momentum flux sometimes develop even if the airflow remains stable and the heat flux is small. Apparently, the reduced stratification allows development of significant shear generation of turbulence. Here, the increase of surface temperature in the downwind direction acts more as a catalyst for shear generation of turbulence in contrast to the convective internal boundary layer where direct buoyancy generation of turbulence is large. More substantial increases of surface temperature, as occurs at the main SST front, lead to significant buoyancy generation of turbulence and warming of the air downwind from the surface front. The resulting horizontal temperature gradient contributes to a local hydrostatic pressure gradient, which accelerates flow towards the warmer air.

The triggering of shear generation of turbulence by modest increases of surface temperature in the flow direction may be much more frequent than the development of convective internal boundary layers downwind from large surface temperature changes. Surface temperature changes over land and sea are often not sufficiently strong to change the sign of the stratification and surface heat flux.

The spatial coverage and sample size in the present data are inadequate for accurate quantitative analysis of the momentum budget and turbulence kinetic energy budgets. Evaluation of the full dynamics of flow past surface temperature changes requires observations of the horizontal variation of the vertical structure of the wind, temperature and fluxes with adequate sampling at each point. This demanding task would be served by a large number of aircraft passes at multiple levels using multiple aircraft and deployment of multiple towers along the track. Otherwise, the interpretation of the data must rely heavily on inferences, as in the present study.

12

Acknowledgements

References

Andreas, E. L., and Cash, B. A.: 1999, 'Convective Heat Transfer over Wintertime Leads and Polynyas', *J. Geophys. Res.* **104**, 25,721-25,734.

Attié, J.-L., and Durand, P.: 2003, 'Conditional Wavelet Technique Applied to Aircraft Data Measured in the Thermal Internal Boundary Layer during Sea-Breeze Events', *Boundary-Layer Meteorol.* **106**, 359-382.

Crescenti, G. H., Crawford, T. L., and Dumas, E. J.: 1999, *Data Report: LongEZ (N3R) Participation in the 1999 Shoaling Waves Experiment (SHOWEX)*. Spring Pilot Study, NOAA Technical Memorandum ERL ARL-232, Silver Spring, MD, 86pp.

French, J. R., Crescenti, G. H., Crawford, T. L., and Dumas, E. J.: 2000, *LongEZ (N3R) Participation in the 1999 Shoaling Waves Experiment (SHOWEX)*, NOAA Data Report OAR ARL-20, Silver Spring, MD, 51pp.

Friehe, C. A., W. J. Shaw, D. P. Rogers, K. L. Davidson, W. G. Large, S. A. Stage, G. H. Crescenti, S. J. S. Khalsa, G. K. Greenhut, and F. Li: 1991, 'Air-sea fluxes and surface layer turbulence around a sea-surface temperature front', *J. Geophys. Res.* **96**, 8593-8609.

Garratt, J.R.: 1987, 'The stably stratified internal boundary layer for steady and diurnally varying offshore flow', *Boundary-Layer Meteorol.* **38**, 369-394.

Garratt, J.R.: 1990, 'The Internal Boundary Layer - A Review', *Boundary-Layer Meteorol.* **50**, 171-203.

Klipp, C. and Mahrt, L.: 2003, 'Conditional Analysis of an Internal Boundary Layer', *Boundary-Layer Meteorol.* **108**, 1-17.

Mahrt, L.: 1982, 'Momentum balance of gravity flows', *J. Atmos. Sci.* **39**, 2701-2711.

Mahrt, L.: 2000, 'Surface Heterogeneity and Vertical Structure of the Boundary Layer', *Boundary-Layer Meteorol.* **96**, 33-62.

Smedman, A., Bergström, H., and Högström, U.: 1995, 'Spectra, Variances and Length Scales in a Marine Stable Boundary Layer Dominated by a Low Level Jet', *Boundary-Layer Meteorol.* **76**, 211-232.

Steyn, D. G. and Oke, R. R.: 1982, 'The Depth of the Daytime Mixed Layer at Two Coastal Sites: A Model and its Validation', *Boundary-Layer Meteorol.* **24**, 161-180.

Sun, J., Vandemark, D., Mahrt, L., Vickers, D., Crawford, T., and Vogel, C.: 2001, 'Momentum Transfer over the Coastal Zone', *J. Geophys. Res.* **106**, 12,437-12,488.

Vickers, D., Mahrt, L., Sun, J., and Crawford, T.: 2001, 'Structure of Offshore Flow', *Mon. Wea. Rev.* **129**, 1251-1258.

Vihma, T. and Brümmer, B.: 2002, 'Observations and Modelling of the On-Ice Air Flow over the Northern Baltic Sea', *Boundary-Layer Meteorol.* **103**, 1-27.